Marine Geology xxx (2016) xxx–xxx

Contents lists available at ScienceDirect

Marine Geology

journal homepage: www.elsevier.com/locate/margo

Sedimentary impacts of recent moderate earthquakes from the shelves to the basin floor in the western Gulf of Corinth

Arnaud Beckers [a,b,*], Christian Beck [b], Aurelia Hubert-Ferrari [a], Jean-Louis Reyss [c], Clément Mortier [a], Paola Albini [d], Andrea Rovida [d], Anne-Lise Develle [e], Efthymios Tripsanas [f], Dimitris Sakellariou [g], Christian Crouzet [b], Oona Scotti [h]

[a] Dept of Geography, University of Liège, allée du 6 août 2, 4000 Liège, Belgium
[b] ISTerre, CNRS UMR 5275, University of Savoie, F-73376 Le Bourget du Lac, France
[c] LSCE, CNRS UMR 8212, avenue de la Terrasse, 91198, F-91191 Gif-sur-Yvette, France
[d] Istituto Nazionale di Geofisica e Vulcanologia, Via E. Bassini, 15, 20133 Milano, Italy
[e] EDYTEM, University of Savoie/CNRS, Le Bourget du Lac, France
[f] Shell U.K. Limited, London, United Kingdom
[g] Institute of Oceanography, Hellenic Center for Marine Research, GR-19013 Anavyssos, Greece
[h] Institut de Radioprotection et de Sûreté Nucléaire (IRSN), Fontenay-aux-Roses, France

ARTICLE INFO

Article history:
Received 28 October 2015
Received in revised form 30 September 2016
Accepted 29 October 2016
Available online xxxx

Keywords:
Paleoseismology
Macroseismic intensity
Event deposits
Turbidite
Sediment density flows
Tsunami

ABSTRACT

In seismically active areas, long term records of large earthquakes are indispensable to constrain reccurence patterns of large earthquakes. In the western Corinth Rift, one of the most active areas in Europe in terms of seismicity, data about ancient earthquakes are still insufficient, despite historical records covering the last two millenia and several studies in onshore paleoseimology. In this paper, we test the use of offshore sediments from the Gulf of Corinth to identify sediment failures and tsunamis that have been triggered by historical earthquakes. Two shelves (40–100 m deep), one sub-basin (180 m) and the basin floor (330 m) have been sampled by short gravity cores. The cores were analyzed in order to identify and characterize event deposits. The age control has been provided by ^{137}Cs and ^{210}Pb activity measurements showing that the cores represent 2 to 4 centuries of sedimentation. In each site, sandy event deposits are interbeded in the muddy, hemipelagic sedimentation. The age of event deposits has been compared to the record of historical earthquakes using new and published macroseismic data. This comparison shows temporal coincidence of some event deposits and documented earthquakes with a macroseismic intensity ≥ VII in the area, e.g. in 1861 CE, 1888 CE and 1909 CE. In nearshore, shallow-water settings, the record of event deposits does not exactly fit with the historical record of large earthquakes because too few event deposits are present. This may be due to the absence of sediment failures or to a lower preservation of the deposits in such settings. In the deepest site, in the basin floor, the correspondence is better: a sandy turbidite probably corresponds to each large earthquake since 1850 CE, except one aseismic sediment density flow that occurred at the end of the 20th century. Surprisingly, the Ms = 6.2, June 15, 1995 Aigion earthquake is only possibly recorded in one nearshore site on the Aigion Shelf, in the form of a tsunami back-wash flow deposit. This study showed that moderate earthquakes (M 5.8–6.5) can significantly impact marine sediments. Regarding the evaluation of seismic hazard in the area, the basin floor is proposed as a promising site for long term paleoseismology in the Gulf of Corinth, while shallower settings need to be considered more carefully.

1. Introduction

In areas where active faults are known or suspected, characterization of past earthquakes is essential to constrain fault activity and to estimate the return periods of their associated seismic cycles. In some parts of the world, historical data provide valuable information about past earthquakes. However, they usually cover a period that is too short to infer the recurrence time of large earthquakes and if they do cover a long enough period, they should include sufficient events in order to make a statistically sound evaluation (Mchugh et al., 2006; Stein et al., 2012). Investigation of the geological record is consequently indispensable to establish the past activity of faults. Compared to terrestrial records, offshore and lacustrine records can have a higher potential for good preservation, a more continuous spatial coverage and a longer temporal span (Goldfinger, 2009). Indeed, numerous processes potentially triggered by earthquakes may have left traces in offshore or

* Corresponding author at: Dept of Geography, University of Liège, allée du 6 août 2, 4000 Liège, Belgium.
E-mail address: abeckers@ulg.ac.be (A. Beckers).

http://dx.doi.org/10.1016/j.margeo.2016.10.018
0025-3227/

lacustrine sedimentary records: subaqueous landslides (e.g. Strasser et al., 2006), turbidity currents (Gràcia et al., 2010; Goldfinger, 2011; Drab et al., 2012; Pouderoux et al., 2012; Moernaut et al., 2014), seiche-effects (e.g. Beck et al., 2007), soft-sediment deformations (e.g. Moernaut et al., 2009Moernaut et al., 2011), creation of a fault scarp (Mchugh et al., 2006Mchugh et al., 2015) and tsunamis (e.g. Dawson and Stewart, 2007; Donato et al., 2008; Jonathan et al., 2012). However, some of these processes can occur without any earthquake triggering. For example, sediment density flows can be triggered by coastal or submarine landslides without any earthquake (Talling, 2014), or by flood events (Mulder et al., 2003). The same is true for coarse-grained layers identified on continental shelves as "event deposits", which can be triggered by storms ("tempestite"), floods, or by tsunamis not caused by an earthquake. Consequently, improving our ability to discriminate earthquake-triggered from non-earthquake-triggered deposits is essential to be able to read geological records as paleo-earthquake archives (Atwater et al., 2014). Subaqueous paleoseismology has been largely developed in subduction zones, where earthquake magnitudes and average recurrence intervals are relatively large (Goldfinger, 2011; Pouderoux et al., 2012). However, the completeness of those records has been challenged (Sumner et al., 2013; Atwater et al., 2014; Talling, 2014), and the ability of event deposit sequences to record moderate magnitude earthquakes with shorter recurrence intervals has never been tested in detail.

The aim of this paper is to analyze in detail the influence of moderate earthquake shaking on sedimentation in different marine settings, from shelves to basin floor, to identify which location may provide the more complete and reliable earthquake record. The study area is the western Gulf of Corinth, Greece (Fig. 1). It has been chosen because (1) it is a seismic area where damaging earthquakes are known from historical sources covering at least 2000 years, and (2) numerous submarine landslides and up to 10 m high tsunami waves, associated with or without earthquakes, have been reported (Galanopoulos et al., 1964; Papatheodorou and Ferentinos, 1997; Papadopoulos, 2000; Ambraseys, 2006; Stefatos et al., 2006). Moreover, the area has been instrumented for 20 years for seismological purposes (Corinth Rift Laboratory, http://crlab.eu/). It is consequently a valuable laboratory for paleoseismological studies. Short gravity cores (<1 m) were retrieved at different water depths in order to investigate the occurrence of sediment density flows in the western Gulf of Corinth during the last three to four centuries. Sedimentological observations are compared to published earthquake catalogues and recent updates concerning large earthquakes of the 19th century (Albini et al., 2014) to discuss in detail the possible imprints of earthquakes on the offshore sedimentation, from the shelves to the basin floor. It is well known from the literature that in this particular setting, submarine landslides are frequent and are not necessarily triggered by earthquakes (e.g. Papadopoulos, 2003). Consequently, turbidite paleoseismology is not expected to be easily used in this area. Several attempts to do classical onshore paleoseismology by trenching during the last decades only gave limited results, partially because most of the faults in the Corinth Rift are located offshore, on the coast, or are blind (i.e. the 1995 Aigion earthquake). It is consequently valuable to test if offshore paleoseismology could be possible.

2. Physical setting and previous works in paleoseismology

The Gulf of Corinth is located in central Greece and separates continental Greece to the north from the Peloponnese to the south (Fig. 1A). This 120 km long sound is connected to the Mediterranean Sea at its western tip through the 62 m deep, 2 km wide Rion sill. The Gulf is the widest (~30 km) and the deepest (~870 m) in its central part. The water depth decreases gradually to the west until the Rion sill (Fig. 1B), while to the east it decreases more abruptly. This study focuses on the western part of the Gulf of Corinth, between the Mornos River fan-delta to the west and the Selinous River fan-delta to the southeast (white box in Fig. 1B). In this section of the Gulf, the relatively flat deep gulf basin plain is gently dipping to the east and is bordered to the south by 300 to 400 m high Gilbert deltas, whose fronts are dissected by numerous gullies (see a 3D view of those deltas in Lykousis et al., 2009, their Fig. 5, and our Fig. 2). The water depth in the basin plain ranges from 90 m at the foot of the Mornos River prodelta to ca.

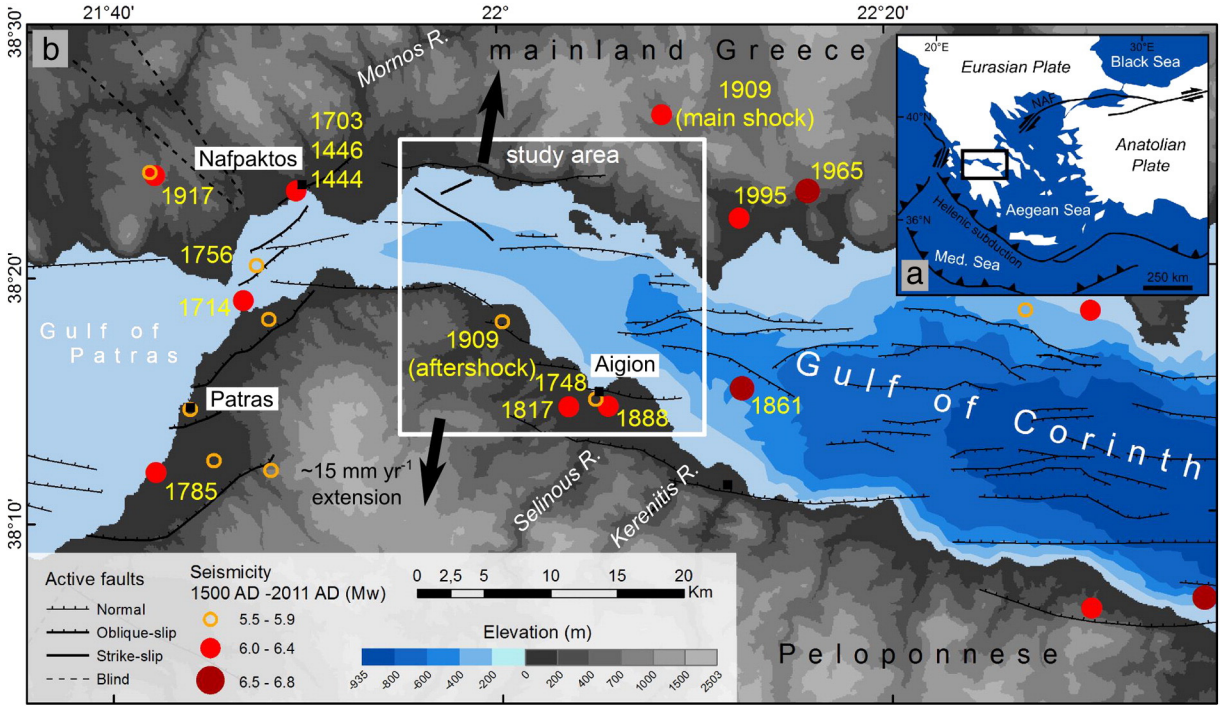

Fig. 1. Tectonic and physical setting of study area, highlighted by the white box in (b). Historical earthquakes from Boiselet (2014). Active faults, i.e. faults with indication of activity during the Holocene, in the Corinth rift and in the Gulf of Patras from Ferentinos et al. (1985), Flotté et al. (2005), Leeder et al. (2005), Bell et al. (2009), Taylor et al. (2011), Beckers et al. (2015) and reference therein. Bathymetry adapted from Bell et al. (2009), elevation from SRTM (http:// http://srtm.usgs.gov/).

Please cite this article as: Beckers, A., et al., Sedimentary impacts of recent moderate earthquakes from the shelves to the basin floor in the western Gulf of Corinth, Marine Geology (2016), http://dx.doi.org/10.1016/j.margeo.2016.10.018

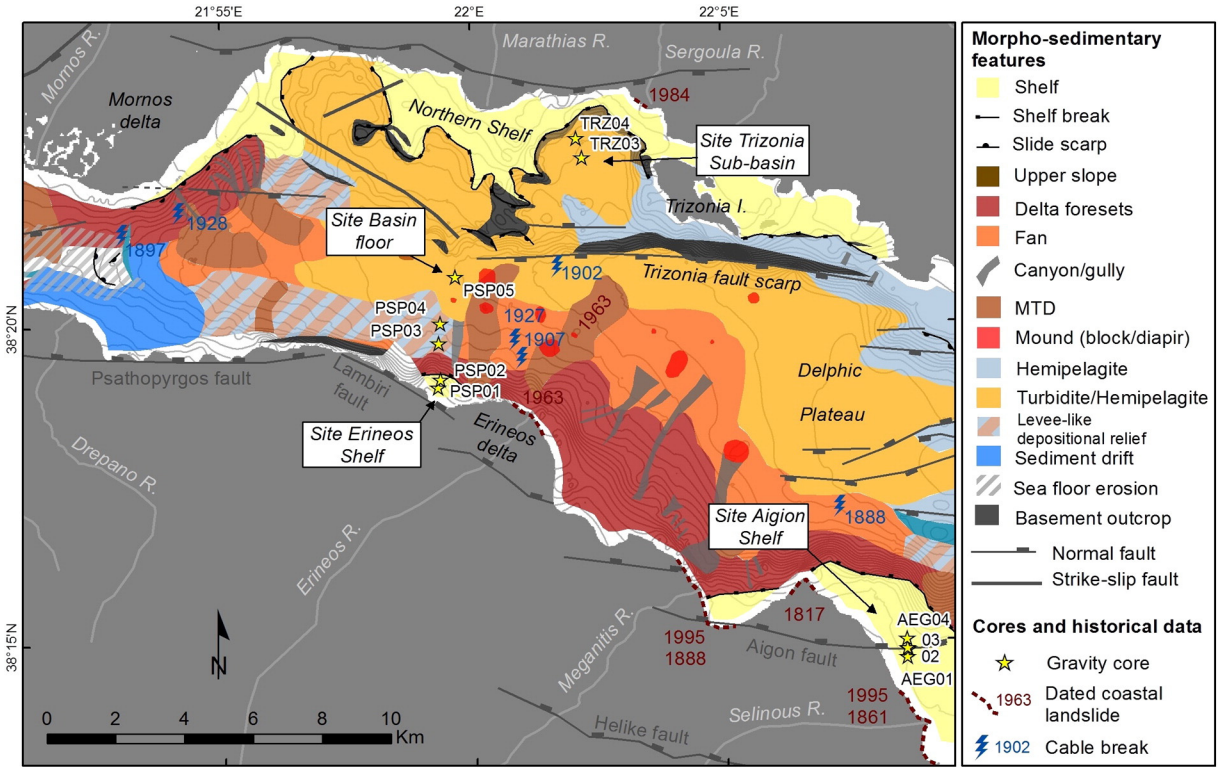

Fig. 2. Core location and morphosedimentary units at the sea floor. Morphosedimentary units from Beckers et al. (2016), faults from Beckers et al. (2015) and references therein, cable break from Heezen et al. (1966), dated coastal landslides from De Martini et al. (2007) and Papadopoulos (2003).

400 m at the foot of the Selinous River prodelta. The northern slope is marked by two sub-horizontal levels (Fig. 2). The shallowest is a 100 m deep shelf and corresponds to the top of ancient deltas built during the last glacial maximum (LGM) (Beckers et al., 2015). The intermediate level, at 170–190 m corresponds to sedimentary sub-basins surrounded by basement culminations and south-facing LGM delta foresets (e.g. the Trizonia Sub-basin). Fault scarps separate this intermediate level from the basin plain.

The western Gulf of Corinth is in the most active part of the Corinth rift, characterized by strong N-S extension. The Corinth rift has been proposed to be the result of a large-scale back-arc extension zone behind the Hellenic Trench, combined with a more localized shearing zone at the western tip of the North Anatolian fault (Fig. 1A) (Armijo et al., 1996; Jolivet, 2001; Hubert-Ferrari et al., 2003; Armijo et al., 2004; Kokkalas et al., 2006; Reilinger et al., 2010; Reilinger et al., 2012). The rift opens at a rate reaching ~15 mm yr^{-1} at its western tip according to GPS measurements (Briole et al., 2000,2004). In this area, the deformation is assumed to be mainly accommodated by north-dipping normal faults bounding the southern edge of the Gulf (Bernard et al., 2006) but offshore normal and strike-slip faults have been mapped as well (Beckers et al., 2015) (Fig. 2). At depth, the analysis of microseismicity revealed a low-angle north-dipping structure (20°–30°) between 7 and 10 km on which steep north-dipping faults could take root (Rigo et al., 1996; Lambotte et al., 2014). This structure has been interpreted as a regional-scale detachment (Rigo et al., 1996; Sorel, 2000; Sorel, 2005; Sorel, 2010) but this interpretation is debated (Hatzfeld et al., 2000; Westaway, 2002; Skourtsos and Kranis, 2009; Bell et al., 2011; Boiselet, 2014; Lambotte et al., 2014).

Many damaging earthquakes have struck the western Gulf of Corinth in the last centuries (Papazachos and Papazachou, 2003) (Fig. 1). The largest reported event is likely the 1861 CE, M_w 6.5 Aigion earthquake that activated the Helike fault (Fig. 1B, Roberts and Koukouvelas, 1996). Many liquefaction phenomena, ground cracks, as well as a 2 m high tsunami wave and coastal landslides have been reported during this earthquake that affected the southern and the northern coast of the Gulf of Corinth (Schmidt, 1879). More recently, the M_w 6.2, 1995 Aigion earthquake has been associated with a north-dipping offshore blind fault (Bernard et al., 1997; Lambotte et al., 2014). The earthquake also triggered submarine landslides and a small tsunami (Papatheodorou and Ferentinos, 1997; Papadopoulos, 2003). Beside the 1861 CE and 1995 CE earthquakes, at least seven other M ≥ 6 earthquakes are known in the area of the western Gulf of Corinth from historical sources since 1600 CE (Papadopoulos, 2000, our Fig. 1B). The last major earthquake sequence activated blind normal faults located under the northern margin of the Gulf (the 2010 Efpalio sequence, Sokos et al., 2012). The 1995 and 2010 earthquakes consequently show that large earthquakes are not necessarily associated with major faults having a surface expression, onshore or offshore.

Submarine or coastal landslides triggered by both earthquakes and other mechanisms are frequent and have been recorded by submarine telegraph cable breaks during the period 1884–1939 CE (Heezen et al., 1966). Landslides often are the triggers of tsunamis in the Gulf of Corinth (Galanopoulos et al., 1964; Stefatos et al., 2006; Tinti et al., 2007). Just like for earthquakes, past tsunamis are known for the last two millennia in the western Gulf of Corinth from historical sources, but only for a few cities and there are certainly gaps in the tsunami record. Geological investigations have consequently been done to improve the earthquake and tsunami catalogues.

Onshore, trenches have been dug on the Aigion and Helike faults (Koukouvelas et al., 2001; Pantosti et al., 2004; Pavlides et al., 2004; Koukouvelas et al., 2005). They allowed an estimation of a maximum recurrence time of 360 yr for large earthquakes on the Aigion fault (Pantosti et al., 2004), and highlighted an increase in slip rate for the Helike fault during the late Holocene, associated with a cluster of four earthquakes between 1000 BCE and 0 (Koukouvelas et al., 2005). Tsunami deposits have been searched for onshore in the western Gulf at four different sites (Kontopoulos and Avramidis, 2003; De Martini et al., 2007; Kortekaas et al., 2011). The longest record has been found in the Aliki lagoon, close to the Aigion fault. Up to 5 possible tsunami layers

Please cite this article as: Beckers, A., et al., Sedimentary impacts of recent moderate earthquakes from the shelves to the basin floor in the western Gulf of Corinth, Marine Geology (2016), http://dx.doi.org/10.1016/j.margeo.2016.10.018

have been described there, dated from 2700 BCE (Kontopoulos and Avramidis, 2003) to 1817 CE (Kortekaas et al., 2011).

Offshore, earthquake-triggered submarine landslides have been studied by Papatheodorou and Ferentinos (1997) and Lykousis et al. (2009). Papatheodorou and Ferentinos (1997) studied four submarine or coastal failures triggered by the 1995 Aigion earthquake. They identified liquefaction deposits (1–2 cm thick sand sheet) offshore, on the rotated blocks belonging to the landslide, as well as onshore, along ground cracks parallel to the shoreline. These observations, as well as others from Schmidt (1879), suggest that liquefaction is a major triggering mechanism for coastal/submarine landslides in the Gulf of Corinth. Papatheodorou and Ferentinos (1997) distinguished different sediment failure processes: multiblock rotational slides, sediment gravity flows, and low-angle translational slides. The presence of gas in the Holocene sediments could have played a role in the sediment failures (Papatheodorou and Ferentinos, 1997; Lykousis et al., 2009). Concerning the location of the slope failures in the western Gulf, the slopes of the Mornos River prodelta have been proved as very unstable by the normalised soil parameter method (Lykousis, 1990).

Despite the fact that many cores have been taken in the deep Gulf (Heezen et al., 1966; Schwartz and Tziavos, 1979; Lykousis, 1990; Piper et al., 1990; Perissoratis et al., 2000; Lykousis et al., 2007), very little attention has been paid to the identification of earthquake-related deposits. Heezen et al. (1966) reported numerous telegraph cable breaks in the Gulf between 1884 CE and 1939 CE, several of them having been related to earthquakes. Lykousis et al. (2007) identified two coarse-grained layers, 8 cm thick, in short gravity cores from the Delphic Plateau, south of the Trizonia Island. They interpreted these layers as turbidites potentially triggered by tsunamis because of their composition (well-rounded, terrigenous grains), their basin-wide occurrence and their uniform thickness. The upper layer has been attributed to the 1861 CE earthquake (distal member of a debris flow) or its associated tsunami. Detailed analyses were carried out on 20 m long cores in the Central Gulf, 50 km to the east of the Delphic Plateau (Van Welden, 2007; Campos et al., 2013a). Thirty-six turbidites-homogenites were identified and attributed to earthquake shaking, leading to an estimate of 400 to 500 yr for the recurrence time of major earthquakes in that area (Campos et al., 2013a, 2013b).

In summary, several damaging earthquakes struck the study area in the last centuries and were often accompanied by submarine landslides and tsunamis. Only one study has looked for historical earthquake (before 1950) impacts offshore, and has highlighted a sandy layer in the basin floor possibly due to the 1861 CE earthquake (Lykousis et al., 2007).

3. Data and methods

We followed the classical approach in offshore paleoseismology, which involves (1) coring specific and carefully selected areas that are considered as favorable for the formation and preservation of earthquake-triggered deposits; (2) identifying in the cores layers that differ from the "background" sedimentation, (3) estimating the age of these "sedimentary event deposits" in each core, and (4) comparing this record to the record of historical earthquakes, submarine landslides and tsunamis in the area. Because of the high frequency of earthquakes in the Corinth Rift, it is relatively easy to "find" an earthquake that took place during the age range calculated for a specific event deposit. For this reason, special attention was given to macroseismic intensity data points that are available for some historical and recent earthquakes, in order to evaluate, in each site, which earthquakes are or are not valuable candidates for the triggering of an event deposit, assuming that higher intensities have greater potential to produce slope failures.

3.1. Sampling sites

Four sites have been sampled: two in nearshore, shallow-water areas, one in a 180 m deep sub-basin and one on the 300 to 400 m deep basin floor (Fig. 2). The nearshore settings are assumed to potentially hold a record of past tsunami backwash flows, while the deeper settings are investigated for possible records of turbidity currents linked to earthquake-triggered sediment failures or resulting from the evolution of tsunami backwash flows (e.g. Arai et al., 2013). In order to characterize the morphology and the sedimentary processes active at these locations, high-resolution single-channel seismic reflection profiles were acquired with a Sparker and a 3.5 kHz source by the Renard Center of Marine Geology, Ghent University (see profiles in Fig. 3).

The first site is the Aigion Shelf, a 40 m deep, ~1.5 km wide subhorizontal shelf formed by the coalescing Selinous and Kerenitis deltas (Fig. 2). Four cores, 50 to 61 cm long, were retrieved along a S-N transect crossing the offshore eastern tip of the Aigion fault (Figs. 2 and 3A). Close to the coring sites, numerous pockmarks and sand volcanoes occur on the seafloor probably as a result of fluid escape from the fault zone (McNeill et al., 2007). About 2.4 km southward, debris-flow deposits have been mapped, just in front of the Selinous River mouth (McNeill et al., 2007). A good record of tsunamis exists for this area because of its proximity to the city of Aigion. Tsunamis with maximum wave eight of 2 to 10 m have been reported along the coast in 1996, 1995, 1963, 1861, 1817, 1748 and 1742 CE (Papadopoulos, 2000). Coastal landslides and liquefaction were reported in the area during the 1995 CE and 1861 CE earthquakes (Schmidt, 1879; Papatheodorou and Ferentinos, 1997).

The second site is the Erineos Shelf. This shelf is located 16 km to the north-west, on the footwall of the Lambiri fault (Fig. 2). Two cores were retrieved there. The coring sites are 70 m (PSP01) and 100 m deep (PSP02) and are situated at 350 m and 500 m from the coastline, respectively (Fig. 3C). The core PSP02 is longer (85 cm) than PSP01 (62 cm). Compared to the Aigion Shelf, the slope of the seafloor is steeper, reaching about 10°. The main historical event that occurred in this site is an aseismic coastal landslide that affected the Erineos fan-delta in 1963 CE (Fig. 2) and triggered a tsunami that hit the northern and the southern coasts of the western Gulf (Galanopoulos et al., 1964).

The third site is a 180 m deep sub-basin located west of the Trizonia Island, close to the northern coast (Trizonia Sub-basin, Figs. 2 and 3B). Two cores were retrieved there: TRZ03 (69 cm) and TRZ04 (60 cm). They are situated 600 m apart, with TRZ03 being more distal with respect to the northern shore than TRZ04. The water depth at the coring sites is 185 m for TRZ03 and 180 m for TRZ04. The basin is surounded by steep slopes (5 to 12°) and could potentially hold a record of turbidity currents triggered on these slopes. Concerning tsunamis and submarine landslides, the only reported event is a moderate tsunami that hit the coast near the village of Sergoula in 1984 (Papadopoulos, 2003). The tsunami was caused by a coastal landslide in the Sergoula area (Fig. 2), triggered by a M_w 5.3, 24 km deep earthquake.

The last site is located in the deepest part of the western Gulf, on the basin floor (Figs. 2 and 3C). One 66 cm long core, PSP05, was retrieved at a depth of 330 m. Frequent turbidity currents are known in this area from previous studies (Heezen et al., 1966; Piper et al., 1988). The turbidity currents potentially come from the Mornos delta to the west, from the Trizonia fault scarp to the north, and from the Erineos delta to the south (location in Fig. 2). Sediment density flows broke telegraphic cables near the coring site in 1928, 1927, 1907, 1902 and 1897 (Heezen et al., 1966; Fig. 2). Among them, only the one that occurred in 1902, on 10th September, was related to an earthquake, according to Heezen et al. (1966). However, no earthquake occurred at this date according to the catalogue we have used (see details about the catalogue in the Section 3.4). The last event that may have affected the coring site is the 1963 landslide in the Erineos fan-delta (Fig. 2).

Finally, two cores were also retrieved on levee deposits on the foot of the Erineos fan-delta (PSP03, 86 cm long and PSP04, 64 cm long), to

Please cite this article as: Beckers, A., et al., Sedimentary impacts of recent moderate earthquakes from the shelves to the basin floor in the western Gulf of Corinth, Marine Geology (2016), http://dx.doi.org/10.1016/j.margeo.2016.10.018

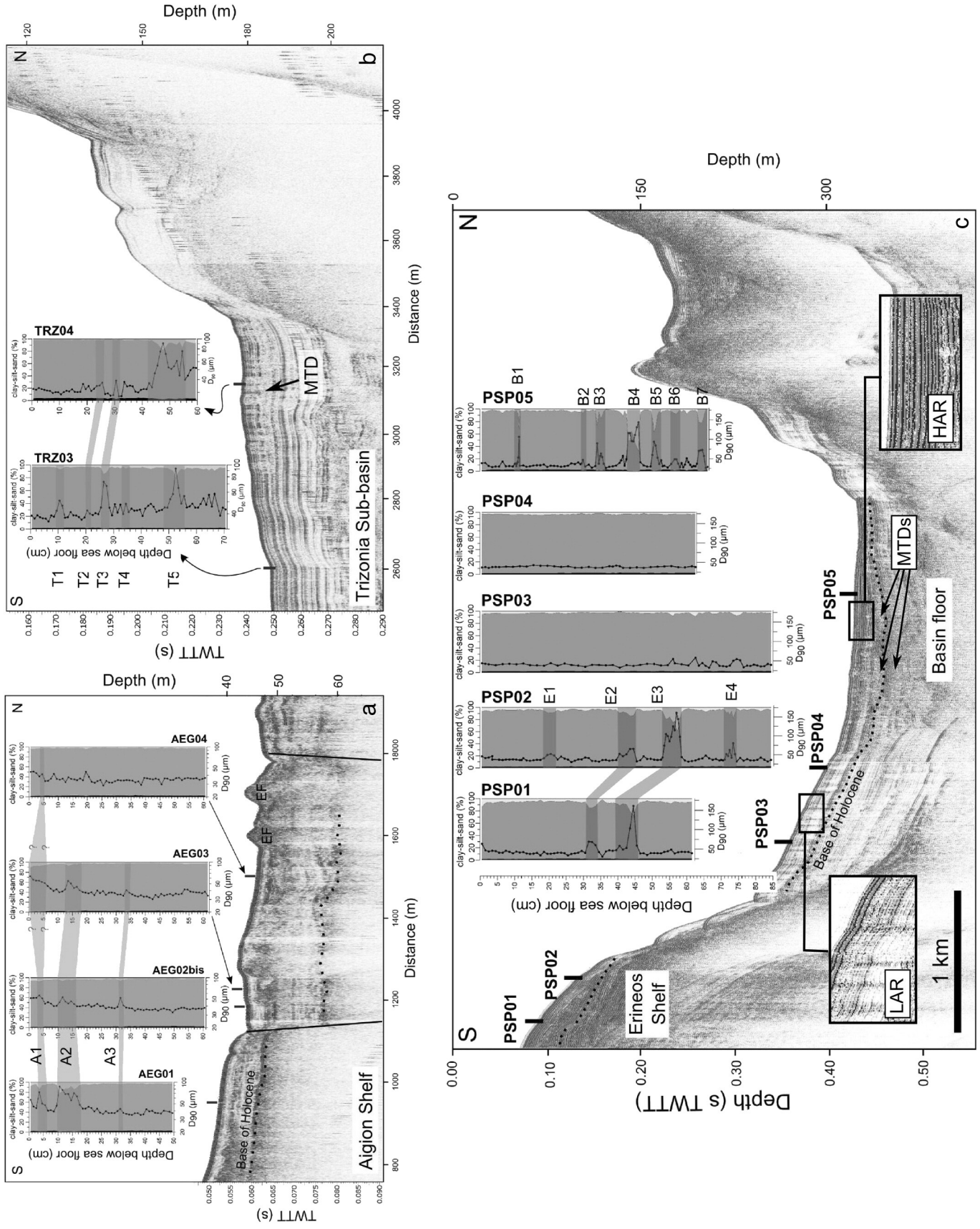

Please cite this article as: Beckers, A., et al., Sedimentary impacts of recent moderate earthquakes from the shelves to the basin floor in the western Gulf of Corinth, Marine Geology (2016), http://dx.doi.org/10.1016/j.margeo.2016.10.018

check the ability of this type of environment to record traces of turbidity currents (Fig. 2).

3.2. Sediment analysis

Sedimentological analyses were performed on each core in order to highlight event deposits that could result, directly or indirectly, from earthquake shaking. X-ray radiography was done on each core on one split half in order to identify sedimentary structures. Grain-size was measured by laser diffraction method (MasterSizer 2000®) with a variable sampling step of 10 to 2 mm. We used 4 μm as the boundary between clay and silt in the representation of grain-size as percentages of clay, silt and sand. Magnetic susceptibility measurements were carried out with a Bartington MS2E Core Logging Sensor each 5 mm. X-ray Fluoresence analysis (XRF) was done on selected cores with an Avaatech® core scanner in the EDYTEM Laboratory, University of Savoie. Each selected core was measured every 2 mm at 10 kV and 30 kV in order to analyze elements from Al to Bi. Among the measured elements, zirconium (Zr) and the silicon/aluminium ratio (Si/Al) were used as proxies for grain-size (e.g. Wilhelm et al., 2013). The calcium/iron ratio (Ca/Fe) and strontium (Sr) were used as proxies for biogenic carbonates (Croudace et al., 2006). We also investigated possible changes in redox conditions through the ratio manganese/titanium (Mn/Ti) and possible human-induced pollution with lead (Pb) and copper (Cu). For each studied core, only the elements and ratios that were used to construct our interpretations are presented. As a non-quantitative technique, XRF core scanner results are expressed as a number of counts for each element. Correlations were measured between grain-size (percentile 90%, i.e. D_{90}) and the number of counts for different elements in order to evaluate the nature of the coarser-grained fraction. The most significant correlations are presented with the correlation coefficient r and the corresponding *p*-value. The use of the median grain-size (D_{50}) instead of the D_{90} gave very similar correlation coefficients, slightly lower in absolute value. Where the interpretation based on these data was difficult, smear slides were prepared from the coarse-grained fraction (≥125 μm) and analyzed with a binocular. It concerns the cores AEG02b and PSP02.

3.3. Age models

Hemipelagic sedimentation rates (i.e. sedimentation rates that do not take the event deposits into account) were accurately assessed for the last century and extrapolated linearly to the base of the core. These recent sedimentation rates were estimated based on unsupported ^{210}Pb ($^{210}Pb_{xs}$) and ^{137}Cs activities measured on 4 cores: AEG02b, TRZ03, PSP02 and PSP05. The cores were sampled every centimeter. Samples were dried and sent to the Laboratoire des Sciences du Climat et de l'Environnement (LSCE) where they were analyzed by gamma counting. Supported ^{210}Pb was assumed to be in equilibrium with the in situ ^{226}Ra activity. $^{210}Pb_{xs}$ was calculated by subtracting ^{226}Ra from total ^{210}Pb. We used the Constant Rate of Supply (CRS) model to derive sedimentation rates from $^{210}Pb_{xs}$ actvities (Appleby and Oldfield, 1978, 1983; Binford et al., 1993). With the CRS model, a sedimentation rate is calculated for each sample, i.e. every 1 or 2 cm in the present case. The model includes the sediment density, allowing to exclude a possible compaction effect. Uncertainties in sedimentation rate were directly derived from the uncertainties in ^{210}Pb activity measurements.

The Gulf of Corinth received ^{137}Cs fall-out during the 1960s atmospheric nuclear bomb tests and after the Chernobyl accident in 1986 (Evangeliou et al., 2013). However, measurements of seafloor sediments in 2007 and 2008 showed very low ^{137}Cs activities (1.1–2.0 mBq g^{-1}) in the western Gulf of Corinth compared to other seas in Greece (Evangeliou et al., 2013). The relevance of using the peaks in ^{137}Cs activities as chronological markers in the Gulf of Corinth is consequently investigated in this study based on sedimentation rates derived from $^{210}Pb_{xs}$ activities.

By extrapolating an average sedimentation rate to hemipelagic intervals downcore, we also extrapolated the associated uncertainties. This gave very large ranges of ages for event deposits located at the base of the cores. To reduce this uncertainty, we tested the use of a particular event deposit that has been observed in every core as an anchor point. This event deposit is dated from the 19th century, and is assumed to be related to a major earthquake. The 1861 CE Aigion earthquake is the largest reported earthquake in and around the study area. This earthquake is the only one with a large surface rupture, and also the only one that induced high macroseismic intensities (larger than or equal to VII), both on the northern and on the southern coast of the western Gulf of Corinth (see the macroseismic map in the Supplementary Materials). It also triggered numerous liquefactions and coastal landslides in the Aigion area (Schmidt, 1879), and a sediment density flow in the basin floor (Lykousis et al., 2007). For these reasons, it is assumed that event deposits associated with this earthquake are widespread in the study area. Consequently, in each core where an event-deposit likely related to this earthquake was found, this event-deposit was used as an anchor point to improve the age-depth curves. Thus, for each coring site, two age-depth curves are presented: the first is only based on $^{210}Pb_{xs}$-derived sedimentation rates while the second uses in addition the 1861 CE sedimentary events as anchor points.

Finally, paleomagnetic measurements were performed at the laboratory of magnetism of CEREGE, University of Aix-Marseille, in order to date sediments using the secular variations of geomagnetic field. Natural remanent magnetization (NRM) was measured on U-channels at 6 to 11 alternating field demagnetization steps with a cryomagnetometer. The characteristic remanent magnetization (ChRM) was extracted by principal component analysis on Zplots using the PuffinPlot software (Lurcock and Wilson, 2012). The parameters of the ChRM were compared to the global model arch3K (Donadini et al., 2009) and a reference curve for the Balkan area (Tema and Kondopoulou, 2011). Unfortunately, this method gave disappointing results, probably because (1) the timespan recorded in our cores is too short to detect these secular variations (the youngest change in geomagnetic feature is dated at around 1775 CE), and (2) the possible action of bottom-currents may affect the orientation of particles (Beckers et al., 2016). However, some correlations between two cores in one site were done based on these magnetic data (Section 4.1.3).

3.4. Earthquake catalogue

In order to compare accurately the sedimentary record to the historical seismicity, we used a recently updated earthquake catalogue for Greece developed by Boiselet (2014), as well as macroseismic data.

Boiselet's (2014) earthquake catalogue is based on Papazachos and Papazachou's (2003) catalogue, updated for ca. 20 earthquakes that occurred in the Corinth Rift area between 1250 CE and 1889 CE (cfr. Boiselet, 2014 p. 94). These updates stem from the reevaluation of published macroseismic intensity data points (MDPs) and from the discovery of new historical sources. This work led to the elimination of some earthquakes from the catalogue, to the reassessment of certain magnitudes, and to changes in some epicenter locations. In order to limit the number of earthquakes that may have triggered sediment failures in

Fig. 3. Seismic profile illustrating each coring site and grain-size for the 11 studied cores. For each core, the fractions of clay, silt and sand are represented in black, grey and light grey respectively. The black lines on top of those plots show the D_{90}. The correlations between event deposits inside each coring site are highlighted in grey. See the core location in Fig. 2 to locate the seismic profiles. A: Aigion Shelf, seismic profile acquired with a 3.5 kHz source. EF = escape feature. B: Trizonia Sub-basin, same source for the seismic profile. C: Erineos Shelf and basin floor, as well as cores PSP03 and PSP04, seismic profile acquired with a sparker source. LHR = low-amplitude reflections, HAR = high-amplitude reflections.

Please cite this article as: Beckers, A., et al., Sedimentary impacts of recent moderate earthquakes from the shelves to the basin floor in the western Gulf of Corinth, Marine Geology (2016), http://dx.doi.org/10.1016/j.margeo.2016.10.018

the study area, we only selected in a first step earthquakes that occurred in the study area (white box in Fig. 1) and within a radius of 25 km around it. The focal depth was also limited to 25 km. For a M_w 6.5 earthquake, this value corresponds to the largest hypocentral distance to get an intensity of VII, according to an attenuation model calibrated for Greece (Papazachos and Papaioannou, 1997). Because widespread subaqueous slope failures generally occur when the macroseismic intensity reaches VII (Schwarz-Zanetti et al., 2003; Monecke et al., 2004; Strasser et al., 2011; Van Daele et al., 2015) and because the largest magnitude for the western Corinth Rift earthquakes is about M_w 6.5 (Boiselet, 2014), this distance threshold is considered as reasonable for the selection of earthquakes around the study area. Such a selection gives a dataset of 225 earthquakes (M_w 4 to 6.5), including 49 earthquakes of magnitude larger than or equal to 5 that occurred between 1600 CE and 2011 CE (Fig. 4).

To refine the analysis, it is interesting to estimate the macroseismic intensity that each earthquake has induced in the areas where the sediment density flows recorded in each core could have been triggered. We called these areas "source areas". They have been delimited manually for each coring site and they comprise every slope and coastal area located upstream of the coring site (Fig. 5). For the nearshore site of the Erineos Shelf, small onland watersheds have also been included in the source area because of the presence of landslides close to the coring site (Palyvos and Pantosti, 2007). Two methods can be used to estimate the macroseismic intensity in the source areas: attenuation modeling and historical reports. Attenuation modeling is based on the location, magnitude, and depth of each earthquake. However, large uncertainties affect those parameters, even for instrumental earthquakes, and they are difficult to quantify. Moreover, we have tested Papazachos and Papaioannou's (1997) attenuation model, and the quality of the fit was highly variable between earthquakes, with errors reaching up to 1–2 intensity units. One likely source of error is the assumption of a point source, that is often necessary because of the difficulty to link historical earthquakes in the Corinth Rift to particular faults (Boiselet, 2014). We consequently chose to only use macroseismic intensities deduced from observations (MDPs) to estimate the intensity of the shaking around each coring site. These data are only available for some large earthquakes. We used Albini et al. (2014) for the 1888, 1861, 1817, 1756, 1714 and 1703 CE earthquakes, Ambraseys and Jackson (1990) for the 1909 CE earthquake, and the ITSAK database for the 1995 Aigion earthquake (http://www.itsak.gr/en/page/data/macroseismic_data/). These macroseismic maps are presented in supplementary materials. They have been established with different macroseismic scales (MSK, EMS-98, MM). Because the different 12-degree macroseismic scales can be considered equivalent (Musson et al., 2010), macroseismic intensities from these sources are indicated without scale in the following. These data were first used to estimate the frequency of earthquakes with intensity ≥ VII in each source area, and then to discuss the possible relation between each event deposit and ancient earthquakes.

4. Results

In this section we present: (1) sediments sampled in the four sites, focusing on the event deposits, and (2) the estimated sedimentation rates. To make our terminology clear, we define here as an event deposit a layer whose sedimentary characteristics (grain-size distribution, structure and/or chemical signature) suggest a more rapid sedimentation process than compared to the background, hemipelagic sedimentation. This rapid sedimentary process can theoretically be associated with a submarine or coastal slope failure, a tsunami, a storm, or a flood. The first two processes can be triggered by an earthquake or by an alternative mechanism. The term turbidite refers here to a normally graded deposit. We use it as a descriptive term, and not genetic.

4.1. Sedimentation and event deposits

4.1.1. The Aigion Shelf

The seismic profile shows that the shelf is marked by fluid escape structures in the hanging wall of the Aigion fault (Fig. 3A). These features possibly influence the sedimentation at core locations AEG02, 03 and 04. Visually, the four cores are composed of very homogenous greenish-brown silt. Grain-size analysis confirms the high silt content and allowed the identification of 3 coarser layers interpreted as event deposits (A1, A2 and A3, Figs. 3A and 6). The correlations between grain-size (D_{90}) and XRF data indicate that the coarser fraction is mainly made of calcareous grains (Ca, $r = +0.37$, p-value $= 0.003$), possibly biogenic (Sr, $r = +0.44$, p-value $= 0.0004$), as well as of terrigenous grains (Zr, $r = +0.32$, p-value $= 0.012$). X-ray pictures show gaps without sediment at different depth, indicating bioturbation by burrowing animals (Fig. 7). The main sedimentary structure imaged on x-radiographs is a slump-like feature between 12 and 16 cm in AEG02b, in the second event deposit (A2). In the same core, the $^{210}Pb_{xs}$ curve does not show the regular exponential decrease expected in constant activity-constant sedimentation rate conditions. A sharp decrease in $^{210}Pb_{xs}$ activity occurs at 6 cm, at the base of the upper event deposit A1 (Fig. 7).

A1 has been identified in AEG01, AEG02b, AEG03 and possibly in AEG04. Delimited from grain-size profiles, it is a 1 to 6 cm thick sandy

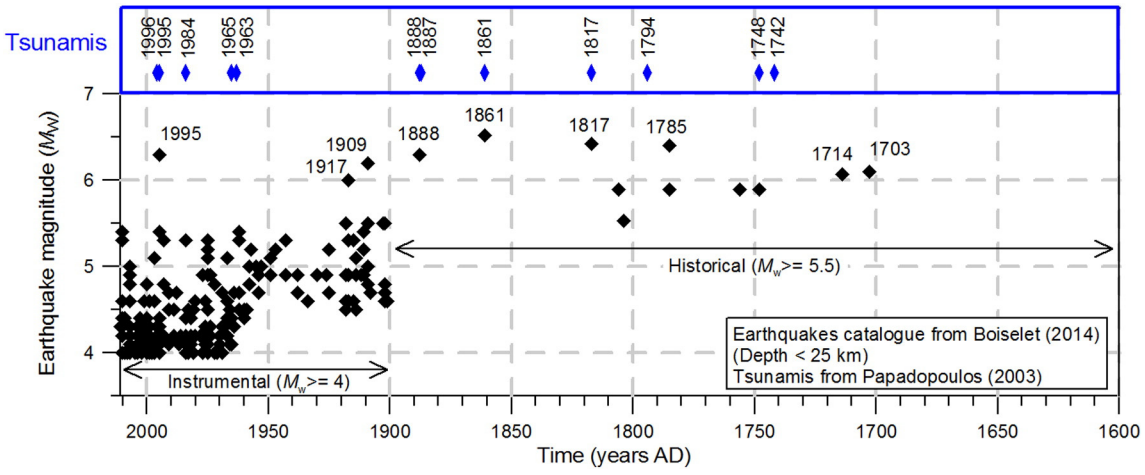

Fig. 4. Earthquakes and tsunamis having affected the westernmost Gulf of Corinth between 1700 CE and 2011. Earthquake catalogue from Boiselet (2014), selected in the study area (Fig. 1) and in a radius of 25 km around it. Depth max = 25 km.

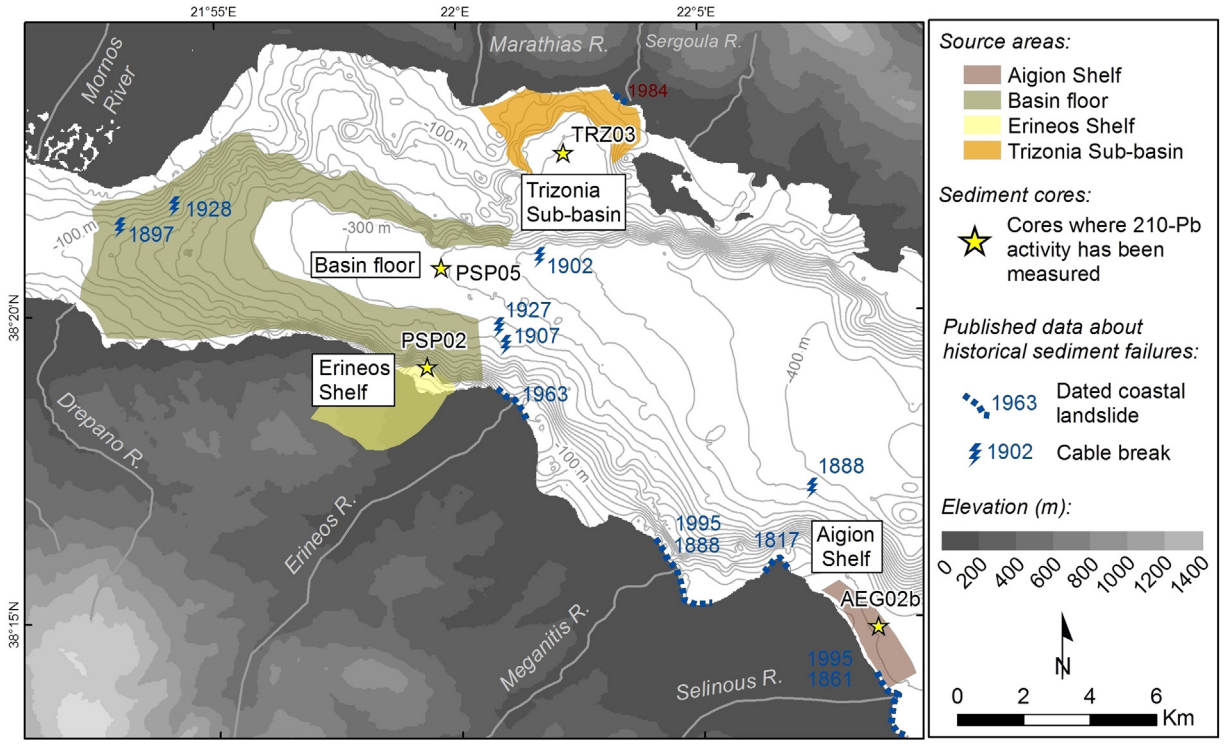

Fig. 5. Source areas for the different coring sites. See the text for explanations.

silt layer made of 5 to 20% of sand, while the hemipelagic sediments contain <5% of sand (Fig. 3A). Its upper boundary is not easy to distinguish in AEG03 and AEG04 (Fig. 3A). In AEG02b, XRF data shows enrichment in Zr/Rb and Ca/Fe (Fig. 7). The first reflects a decrease in Rb, Zr being relatively stable, while the second results from a light increase in Ca combined with a decreasing trend in Fe from ~20 cm to the top of the core. Zr does not show any clear variation along the whole core. The increase in grain-size defining the base of A1 is not sharp. In AEG01, observation with the binocular of the >250 μm fraction showed 42–52% of terrigenous grains and 40–54% of bioclastic grains, as suggested by XRF data. Terrigenous grains are only weakly blunted, indicating a fluvial, and not coastal, transport. Bioclastic grains are mainly *Spatangidae* fragments and fragmented or whole bivalve and gastropod shells, with a few foraminifera. A difference exists in the ratio between fragmented and whole shells. It reaches 15 for a sample belonging to A1 (3–4 cm), and 3.5 for a sample just below (7–8 cm), in sediments interpreted as hemipelagites. The sharp decrease in the $^{210}Pb_{xs}$ activity at 6 cm, just at the base of A1, could indicate seafloor erosion associated with the overlying event deposit.

The second coarser layer A2 has been identified in the cores AEG01, AEG02b and AEG03. Its thickness decreases seaward from 7 to 4 cm (Fig. 3A). The slump-like feature on the X-ray photograph between 12 and 16 cm in AEG02b is possibly present in AEG03 as well. The layer is made of two peaks in grain size, the upper one being the more marked. No clear signature in the Zr/Rb or in the Ca/Fe ratio can be observed in the three cores (e.g. Fig. 7 for AEG02b), suggesting a local origin. Observation with a binocular (AEG01, sampling at 11–12 cm) showed numerous shell fragments in the fraction >250 μm, with a ratio fragmented/whole shells of 9.

The last coarser layer A3 is 1 to 2 cm thick and has been clearly identified in AEG02b and AEG03 based on the D_{90} (Fig. 3A), and possibly in AEG01 based on the MS and the Ca/Fe ratio (not shown). It has a significant geochemical signature in AEG02b, similar to the upper event deposit A1 (Fig. 7). However, this signature has not been found in AEG01 neither in AEG03.

4.1.2. The Erineos Shelf

The cores PSP01 and PSP02, located on the Erineos Shelf, are made of grey-brown silt with two and four coarser layers respectively. These event deposits have been detected by the naked eye based on their characteristic texture. Compared to the silty, hemipelagic intervals, these event deposits are composed of dark sandy grains dispersed in a silty matrix that is very similar in colour to the hemipelagic sediments. They are 2 to 5 cm thick and grain-size analysis carried out on both cores show that they contain 10 to 40% of sand (Fig. 3C). Detailed grain-size measurement, XRF and radionuclides measurements have been done on the longest core, PSP02 (Fig. 8), and smear slides were made from E2, E3 and E4. Event deposit E1 is the thinnest (2 cm) event deposit in this core. XRF data shows that, despite an increase in grain-size, the chemical characteristics of this event deposit do not differ from the overlying and underlying hemipelagic sediments (Fig. 8). Between 41 and 45 cm, E2 is thicker and is characterized by sharp increase and decrease in grain-size at the base and at the top of the event deposit, respectively (Fig. 8). Again, XRF data do not show any typical signature. Binocular observation showed that the coarser fraction (>125 μm) is mainly composed of terrestrial plants remains and charcoals (~3/4) with a few forams and shell fragments. A peak in Ca/Fe occurs between E2 and E3, but is not associated with any coarser-grained layer. E3 is the thickest (5 cm) and the coarsest event deposit (Figs. 6 and 8). It is characterized by an increase in Zr/Rb that is due to a decrease in Rb (Fig. 8). The coarser fraction (>125 μm) is made of lithics (~3/4), plant remains (~1/4) and a few fragmented or whole shells. Between 71 and 75 cm, the last event deposit E4 shows a dark-grey sandy base overlain by 2 cm of sediment showing the same facies as the other 3 event deposits. The dark base is enriched in Br, Pb and Fe. Binocular observation showed that ~95% of the grains >125 μm are plant remains.

The correlation of event deposits between PSP01 and PSP02 has been based on the D_{90} (Fig. 3C). In the longest core PSP02, E2 and E3 show a grain-size profile comparable to those of the upper and the lower event deposit in PSP01, respectively. The proposed correlation

Please cite this article as: Beckers, A., et al., Sedimentary impacts of recent moderate earthquakes from the shelves to the basin floor in the western Gulf of Corinth, Marine Geology (2016), http://dx.doi.org/10.1016/j.margeo.2016.10.018

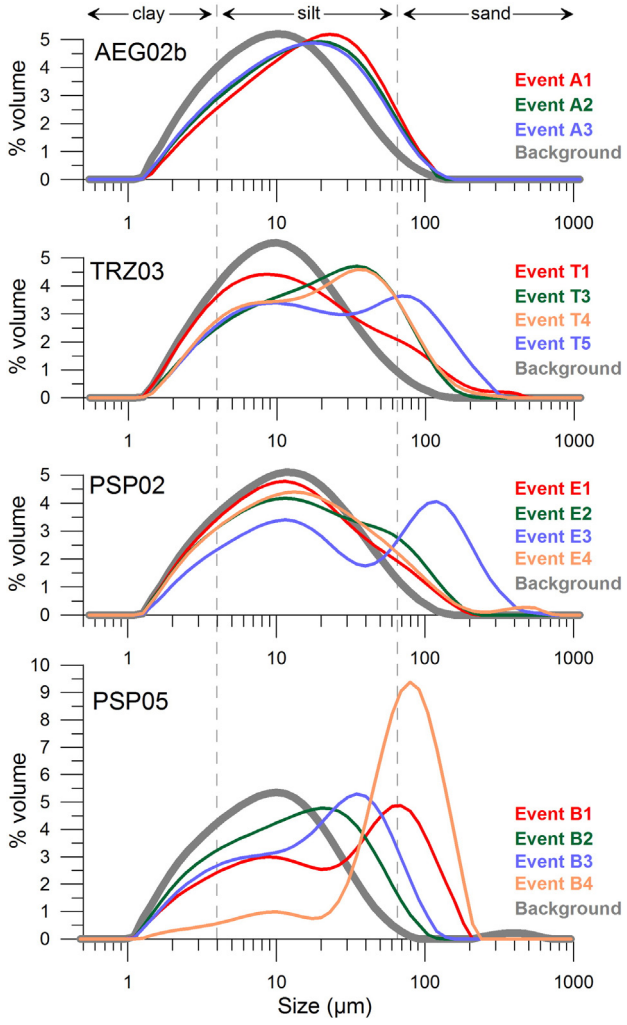

Fig. 6. Grain-size distribution in event deposits and for the "background" sedimentation.

implies that E1 in PSP02 is not detected in PSP01 and that the sedimentation rate in PSP02 is ~30% larger than the one in PSP01.

4.1.3. The Trizonia Sub-basin

Cores TRZ03 and TRZ04 were retrieved in a small basin north of the deep basin floor (Figs. 2 and 3B). Seismic profiling shows that TRZ04 is possibly affected by fluids escaping from an underlying mass-transport deposit, while the sedimentary sequence below TRZ03 appears undisturbed (Fig. 3B). The two cores are made of very homogenous grey-brown silty sediments. The only structures visible to the naked eye are slightly darker convoluted lenses at 24–28 cm in TRZ03 and at 27–32 cm in TRZ04. Detailed observations as well as radionuclide activity measurements have been done on TRZ03 (Fig. 7). The stratigraphy of the Trizonia Sub-basin has been established based on this core, and correlations with core TRZ04 have been tested afterwards.

Four coarser-grained layers were identified in TRZ03 based on detailed visual description and X-radiographies (Fig. 7). The event deposit T2 is made of two 2 mm thick dark-grey sand layers at 19.5 cm that are separated by a 1 mm thick grey-brown silt layer. On the X-ray photograph, these sand layers are imaged as two lighter layers (Fig. 7). Between 23 and 28 cm, event deposit T3 corresponds to the darker convoluted lenses where a few millimeter-scale irregularly shaped sand clasts are dispersed in the silty matrix. On the X-ray photograph, this interval appears bioturbated, with at least 3 lighter levels (Fig. 7). This suggests that the observed convoluted lenses reflect a bioturbated layer containing sand. The same facies is observed between 33 and 36 cm (T4) with sand clasts identified by the naked eye and three to four lighter, sandy (?) layers detected on the X-ray photograph. The last event deposit T5 is an almost continuous 2–3 mm thick fine-sand turbidite at 52.5 cm, which is surprisingly not visible on the X-ray photograph (Fig. 7).

High-resolution grain-size analyses on TRZ03 confirm the four coarse-grained layers described above (T2 to T5, Fig. 7) and highlighted a fifth one (T1) between 11 and 12 cm (Fig. 7). Grain size distribution is bimodal in the event deposits and unimodal for the background sedimentation (Fig. 6). The Zr/Rb ratio is quite noisy but shows an excess in Zr at the depth of T3 and T5 (Fig. 7). Among 19 different XRF elements and ratios tested, Zr/Rb is the only ratio positively correlated with the D_{90} ($r = +0.39$, p-value $= 0.001$), while Ca, Ca/Fe and Ca/Ti are negatively correlated ($r = -0.35$ to -0.40; p-value < 0.005). These correlations indicate that the coarse-grained fraction is mainly composed of terrigenous grains. This particularly concerns the event deposits T3 and T5, in which an excess in Zr is highlighted.

In TRZ04, four possible event deposits have been highlighted by the X-ray radiography and/or by the low resolution (every 10 mm) grain-size measurements (Fig. 9). This core has been correlated to TRZ03 in order to check the spatial extent of the event deposits. Because the XRF profiles did not show clear variations making correlations possible, two magnetic properties have been used to establish the correlation: the magnetic susceptibility (MS) and the inclination of the ChRM. Each parameter allows the definition of one anchor zone. The first is a typical peak in MS corresponding to T1 in TRZ03, while the second is a maximum in the inclination of the ChRM between T3 and T2 in TRZ03 (Fig. 9). This correlation indicates a slightly higher apparent sedimentation rate for TRZ04 as already suggested by the depths of the convoluted lenses described above in the two cores, which correspond to T3. This could have been induced by the likely significant tilt of the corer at the TRZ04 coring site suggested by the apparent tilt of the stratigraphy in X-ray photographs (Fig. 9). Event deposits T2 and T3 can be reasonably correlated between both cores. Assuming that the upper peak in MS in TRZ03 is due to T1, this event deposit seems present in TRZ04 at 12 cm but is not characterized by a coarser grain-size. This could result from the difference in measurement intervals between TRZ03 (2 mm in T1) and TRZ04 (10 mm in the corresponding interval). The absence of reliable anchor point below T3 makes further correlations speculative.

4.1.4. The basin floor

PSP05 is located in the basin floor, 330 m b.s.l. Seismic profiles show high-amplitude reflections on top of lenses of incoherent reflections (Fig. 3C). These two units are interpreted as turbidites and lenses of mass-transport deposits, respectively. The core consists of an alternation of grey-brown silt and seven sandy layers (Fig. 8). The sand fraction varies from ~5% in the background sediments to 10–70% in the event deposits (Figs. 3C and 6). Zr/Rb and Si/Al are positively correlated with grain-size (D_{90}), indicating for each event deposit a terrigenous origin of the sediments (Fig. 10). Event deposit B1 is a 1.5 cm thick, normally graded silt layer overlying a thin sandy base. XRF data shows a high enrichment in Zr/Rb as well as the presence of Cu (Fig. 8). The instantaneous character of B1 is highlighted by lower $^{210}Pb_{xs}$ activities that indicate a higher sedimentation rate or the reworking of older sediments (Fig. 8). About 18 cm below, B2 is a discontinuous, 0.5–1 cm thick normally graded silty layer. We interpret this layer as the bioturbated distal part of a turbidite. Event deposit B3 has a similar thickness but has a higher sand fraction (20–25%) with isolated sandy patches at the top. These features probably correspond to bio-induced holes filled by sand coming from the upper or underlying sand layer. The grading is not clear and could be inverse (Fig. 8). The event deposit has no clear XRF signature. Between 42 and 46 cm, B4 is the thickest event deposit recorded in this core. It is made of a 4 cm thick massive, well-sorted sand bed with an erosive base (Figs. 6 and 8). The grading is normal from the base to 3 cm and then slightly inverse in the last upper cm. The upper boundary is irregular with numerous sandy patches/filled

Please cite this article as: Beckers, A., et al., Sedimentary impacts of recent moderate earthquakes from the shelves to the basin floor in the western Gulf of Corinth, Marine Geology (2016), http://dx.doi.org/10.1016/j.margeo.2016.10.018

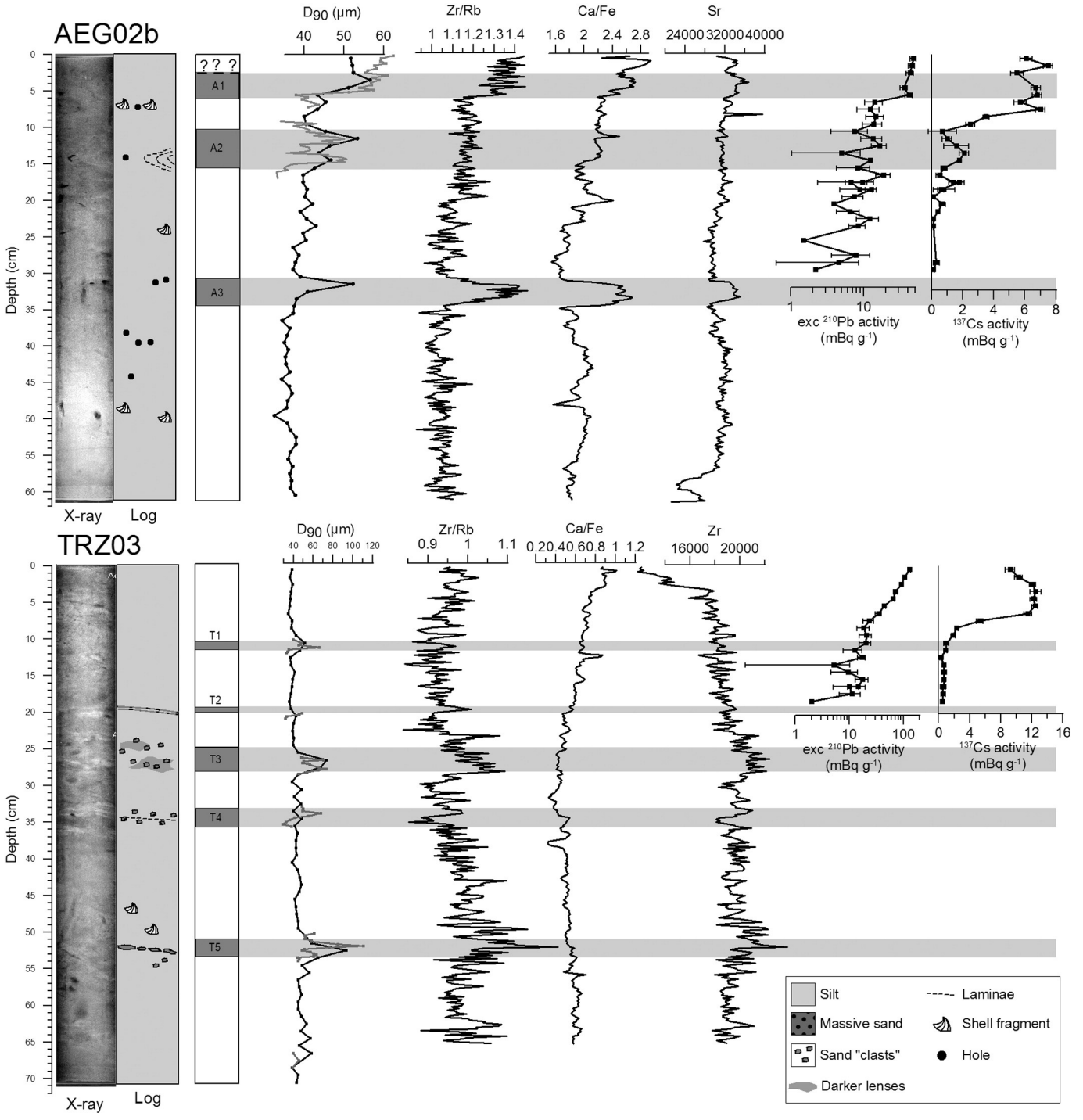

Fig. 7. X-ray pictures, log, event deposit delimitation, grain-size, indicative XRF ratios and radionuclide data for AEG02b and TRZ03.

holes, up to 1 cm in size. Above the sand bed, the absence of structure makes it difficult to differentiate between silty sediments potentially belonging to the event deposit and the background, hemipelagic sedimentation. This remark is also valid for the other event deposits in this core. XRF shows enrichment in Zr and in Cu in the sand bed, similarly to B1. The three deepest event deposits are the most bioturbated, making their characterization in terms of thickness, structure and grading difficult. Event deposit B5 is a ~2 cm thick sandy layer (40% sand) with an irregular shape and sandy patches/filled holes below. The apparent inverse grading is due to the presence of these underlying sandy patches/filled holes. The presence of two peaks of enrichment in Zr has the same origin. Event deposit B6 is a ~1 cm thick deposit relatively fine-grained in comparison with the other event deposits. From the base to the top, grain-size analysis shows an inverse grading followed by a normal grading that may indicate a flood origin (hyperpycnal flow). The deepest event deposit B7 is made of massive sand and has a convoluted structure. Its thickness varies between 0.2 and 3 cm. This irregular structure may be due to post-depositional fluidization or bioturbation. Grain-size varies abruptly at the base and at the top of the event deposit, similarly to event deposit B4.

4.1.5. PSP03 and PSP04

PSP03 and PSP04 have been retrieved at 260 and 300 m b.s.l respectively. The seismic profile in Fig. 3C shows that they are located on

Please cite this article as: Beckers, A., et al., Sedimentary impacts of recent moderate earthquakes from the shelves to the basin floor in the western Gulf of Corinth, Marine Geology (2016), http://dx.doi.org/10.1016/j.margeo.2016.10.018

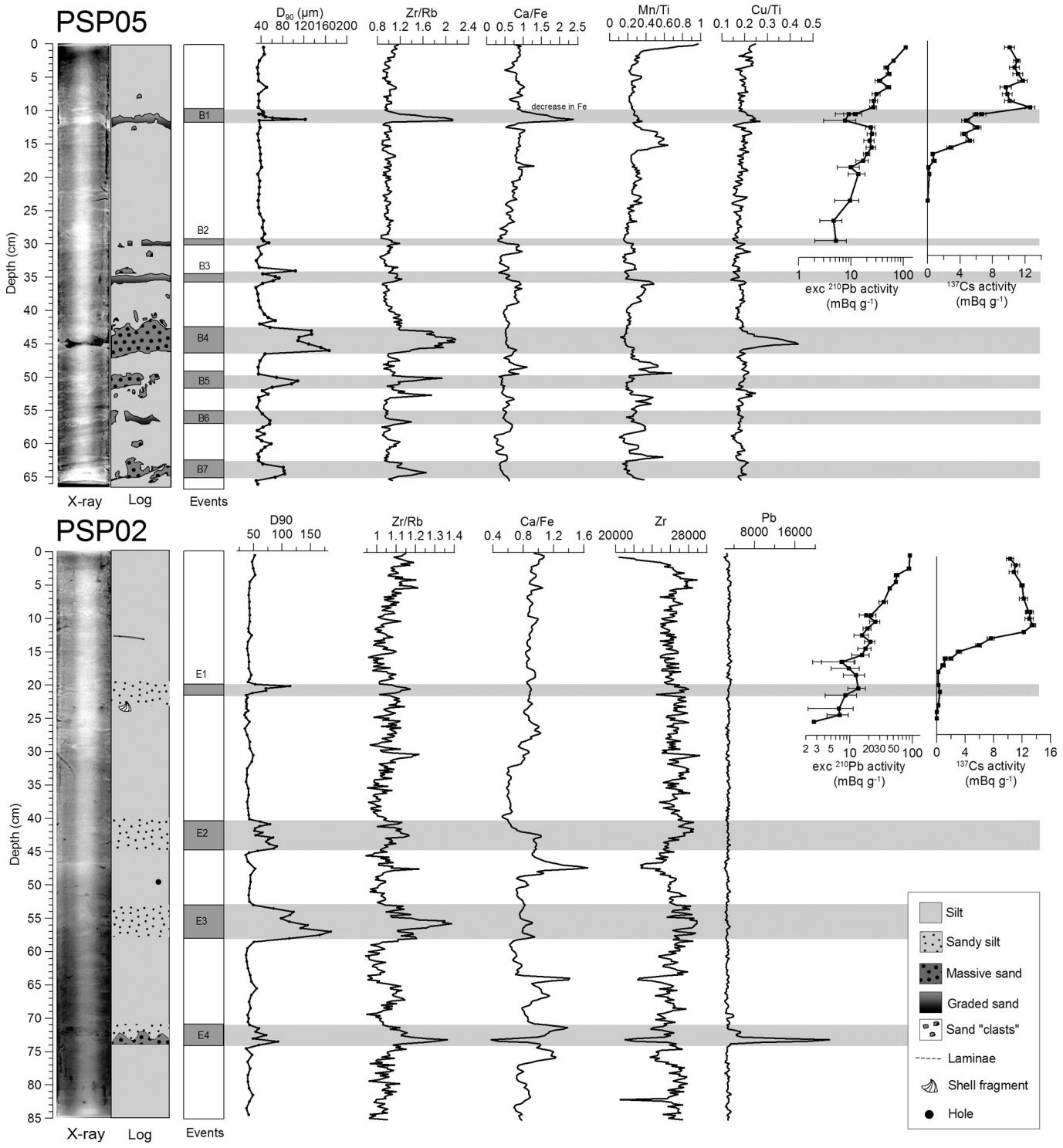

Fig. 8. X-ray pictures, log, event deposit delimitation, grain-size, indicative XRF ratios and radionuclide data for PSP05 and PSP02.

continuous, low-amplitude sub-parallel reflections that have been interpreted as hemipelagites possibly influenced by bottom-currents (Fig. 2; Beckers et al., 2016). The cores are made of homogenous silt, without any coarser-grained level. This homogenous grain-size composition confirms the nature of the sediment body. As proposed by Beckers et al. (2016), the sediment source may be hemipelagic sedimentation, turbidity currents running in the deep gulf (Heezen et al., 1966), and/or tidally-induced bottom-currents passing through the Rion sill. This depositional environment is not the most appropriate for paleoseismological purposes.

4.2. Sedimentation rates

In all the analyzed cores (AEG02, PSP02, TRZ03 and PSP05), $^{210}Pb_{xs}$ activity shows a general exponential decrease with depth, affected by irregularities (Figs. 7 and 8). These irregularities are the largest in AEG02b and PSP05 (Fig. 7) and tend to indicate that the CRS model is the most appropriate for the western Gulf of Corinth data. Moreover, Appleby and Oldfield (1983) proposed that the CRS model gives reasonably accurate results where the total amount of $^{210}Pb_{xs}$ in neighboring cores

Please cite this article as: Beckers, A., et al., Sedimentary impacts of recent moderate earthquakes from the shelves to the basin floor in the western Gulf of Corinth, Marine Geology (2016), http://dx.doi.org/10.1016/j.margeo.2016.10.018

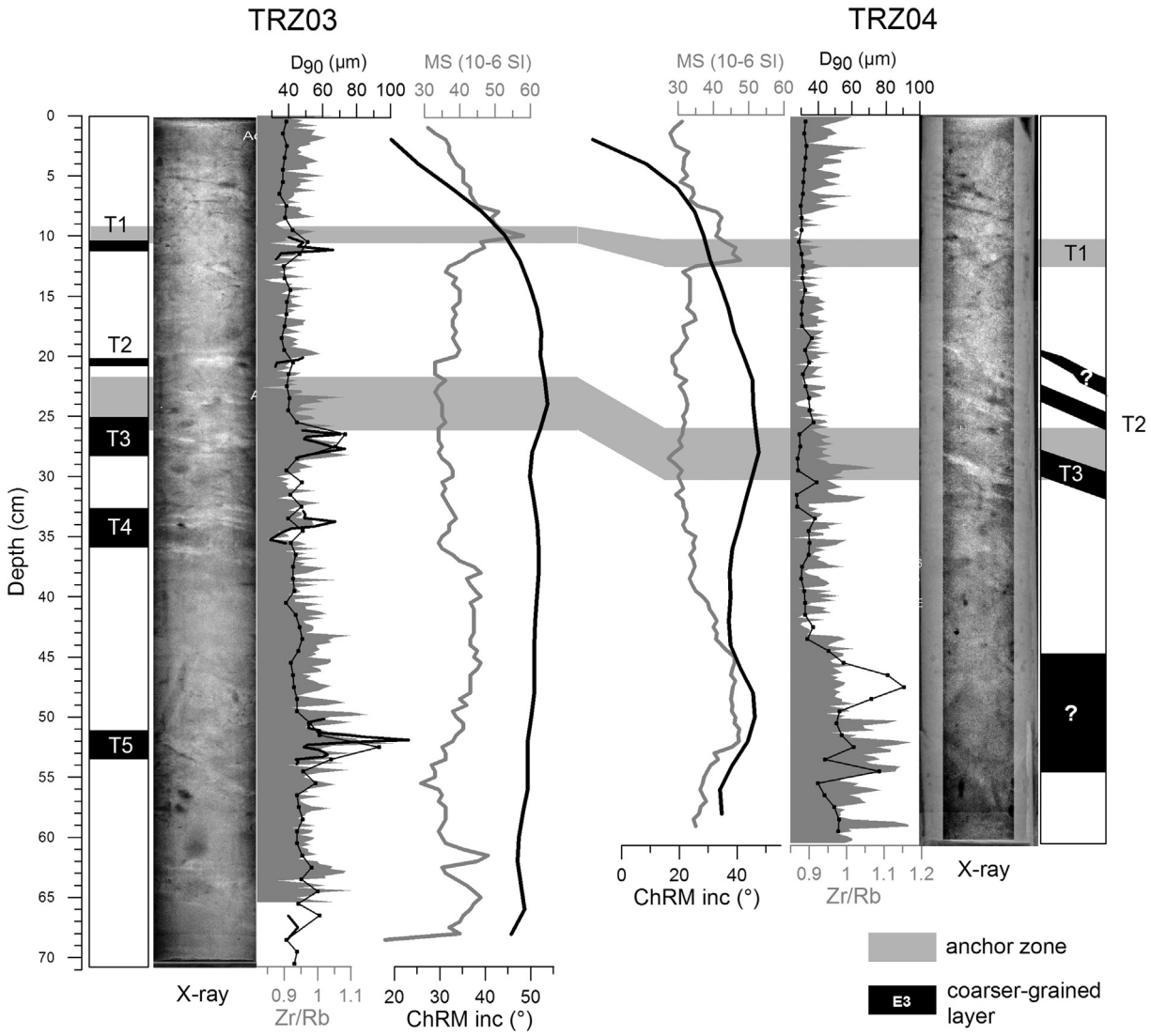

Fig. 9. Examples of correlations between two XRF ratios (ZR/Rb and Si/Al) and grain size (D_{90}) for the core PSP05. A part of the relatively high scattering likely results from millimetric discrepancies between the depths measured by the XRF core scanner and the depths measured during the sampling for grain-size measurement.

is similar. Table 1 shows that this is the case in 3 of the 4 cores, namely PSP02, TRZ03 and PSP05. Average inter-event sedimentation rates derived from the CRS model range from 1.6 to 2.8 mm yr^{-1} for those cores (Table 1). AEG02b shows a significantly lower $^{210}Pb_{xs}$ activity at the surface and lower total residual $^{210}Pb_{xs}$ content. The latter could at least partially result from the erosion observed at 6 cm (Fig. 7), which may have removed a significant part of the total $^{210}Pb_{xs}$ content in that area. Another hypothesis is that the top layer has been eroded, leading to a lower activity at the surface and a lower total residual $^{210}Pb_{xs}$ content. Beside this question of lower $^{210}Pb_{xs}$ activity, the presence of the event deposits A1 and A2 in the upper 20 cm of the profile prevents assessing any reliable inter-event sedimentation rate with a model such as the CRS model.

^{137}Cs data have been added to the $^{210}Pb_{xs}$ profile interpretations. The shape of ^{137}Cs profiles differs between coring sites (Figs. 7 and 8). In PSP02, only one peak is observed at 10 cm. In TRZ03, one peak forms a *plateau* between 3 and 6 cm. In PSP05, 3 peaks exist at 5.5, 9.5 and 12.5 cm, but the profile is possibly disturbed by the sandy turbidite B1 that could induce lower ^{137}Cs activities between 10 and 12 cm (e. g. Alonso-Hernandez et al., 2006). The profile in AEG02b is more complicated with up to 6 local peaks. This variability in ^{137}Cs profiles shape in marine sediments is documented elsewhere in Greece. In the Amvrakikos Gulf, 120 km to the NW, ^{137}Cs has been measured in two cores (Evangeliou et al., 2013). The 1960s peak induced by the nuclear tests appears stronger than the 1986 (Chernobyl event) peak in one core, while the profile of the second core is more difficult to interpret. The shape of the ^{137}Cs profile is different in the Northern Aegean Sea, where a larger and thicker peak has been attributed to the Chernobyl accident (Tsabaris et al., 2012). Based on these two studies, ^{137}Cs profiles from the Gulf of Corinth cannot be interpreted unambiguously independently from $^{210}Pb_{xs}$ results. In PSP02, located close to the southern shore, $^{210}Pb_{xs}$ results date the only peak in ^{137}Cs at 1965 (1958–1971), which corresponds well to the nuclear tests of the 1960s. $^{210}Pb_{xs}$ and ^{137}Cs consequently give the same sedimentation rate in this site (Fig. 11). In TRZ03, close to the northern shore, the lower limit of the *plateau*, which is also the oldest peak in the ^{137}Cs profile, would date from 1972 to 1980 according to $^{210}Pb_{xs}$ results (Fig. 12). A similar range of ages is obtained for the largest ^{137}Cs peak in PSP05 (1973–1982, Fig. 13). For these two cores, if the selected ^{137}Cs peaks actually correspond to the 1960s, the last 50 yr sedimentation rate deduced from the ^{137}Cs profile is slightly smaller than the one deduced from the CRS model. Finally, in AEG02b, even if the $^{210}Pb_{xs}$ and ^{137}Cs activity profiles are difficult to interpret, at least one piece of information can be obtained. Indeed, the absence of ^{137}Cs below 23 cm shows that this depth likely corresponds to 1950–1955 CE, while the absence of $^{210}Pb_{xs}$ below ~30 cm would give an age of about 1910 CE for this

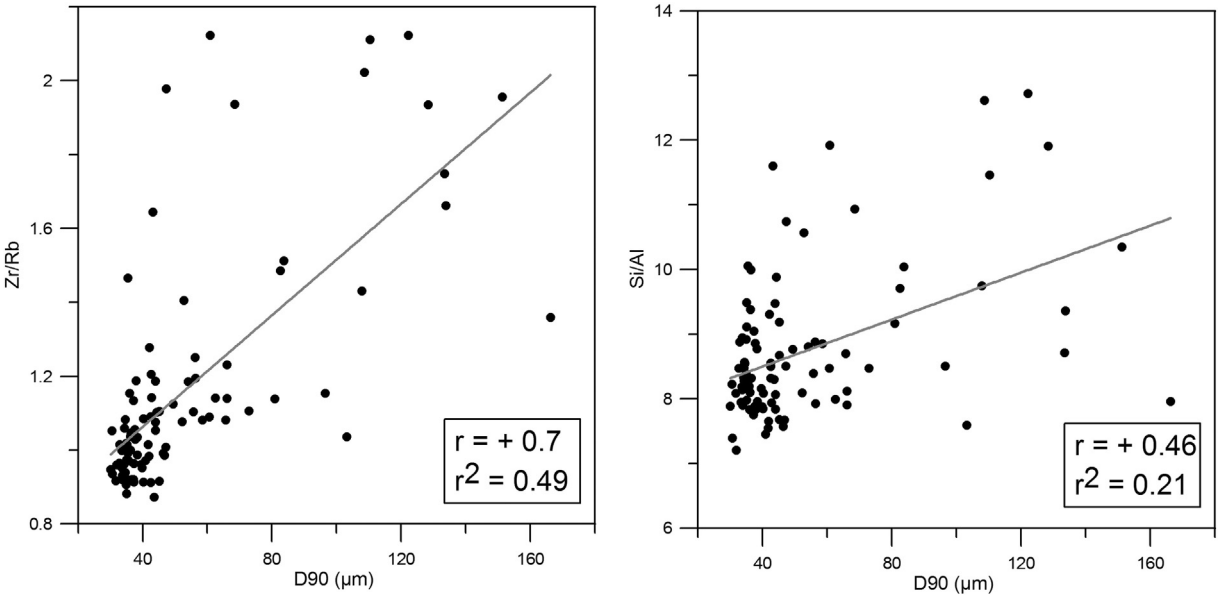

Fig. 10. Proposed correlations between sedimentary events in site 3 based on Natural Remnant Magnetization. The three extrema of the NRM curve highlighted in grey were used for the correlation.

depth. This gives a very rough estimate of about 2–3 mm yr^{-1} for the inter-event sedimentation rate in this core.

In summary, in PSP02, TRZ03 and PSP05, only $^{210}Pb_{xs}$ data have been used to estimate inter-event last century sedimentation rates based on the CRS model (Table 1), because the detailed interpretation of ^{137}Cs profiles is in some cases ambiguous. The age-depth curves deduced from the CRS model for these cores are presented in Figs. 11, 12 and 13. In AEG02b, we used the maximal depths where $^{210}Pb_{xs}$ and ^{137}Cs activities have been detected to propose a rough estimate of the inter-event sedimentation rate.

The sedimentation rates deduced from radionuclide activity profiles can be compared to average Holocene sedimentation rates derived from the interpretation of seismic profiles (Beckers et al., 2015; McNeill et al., 2007) (Table 1). In PSP02 and PSP05, the rates remarkably are in the same order of magnitude. This is not the case in AEG02b, where recent sedimentation rate (2–3 mm yr^{-1}) seems higher than the Holocene rate (1.0–1.5 mm yr^{-1}).

5. Interpretation: age and possible triggering mechanisms for event deposits

In this section, the relationship between event deposits observed in cores and earthquake shaking is discussed. First, we compare the recurrence of both phenomena during the last two to three centuries. Then, each event deposit is interpreted based on its age and based on the phenomena that have been reported during the corresponding period, i.e. earthquakes, submarine landslides or tsunamis.

5.1. Recurrence times for strong earthquake shaking and event deposits

Table 2 shows average recurrence intervals for event deposits occurrence at each coring site and average earthquake frequency. Obviously, similar values of average frequency between large earthquakes and event deposits do not prove that each event has been earthquake-triggered. However, this comparison reveals where the method definitely does not work.

In the Erineos Shelf and in the Trizonia Sub-basin, the number of event deposits varies between neighboring cores. Considering the cores in which the largest number of event deposits has been found, the average recurrence intervals reach 65–75 yr in the Erineos Shelf (PSP02), 62–76 yr in the Trizonia Sub-basin (TRZ03), 57–83 yr in the Aigion Shelf, and 27–37 yr in the basin floor (PSP05). If we only consider the event deposits that have been correlated in each site between two cores, recurrence intervals are significantly longer. They reach 130–150 yr in the Erineos Shelf and 104–127 yr in the Trizonia Sub-basin.

Table 1
Summary of $^{210}Pb_{xs}$ data and associated mean sedimentation rate according to the CRS model. For the core AEG02b, we propose a rough estimate of the sedimentation rate over the last 100 yr based on ^{137}Cs and $^{210}Pb_{xs}$ activity profiles. These recent rates are compared to average Holocene sedimentation rates derived from seismic reflection data interpretation.

				Average sedimentation rates (mm yr^{-1})		
Core	Unsupported total residual ^{210}Pb content (mBq cm^{-2})	Unsupported ^{210}Pb at the surface (mBq g^{-1})	Thickness of Holocene deposits from seismic profiles (m)	Last 50 yr ($^{210}Pb_{xs}$, CRS, hemipelagic intervals)	Last 100 yr (^{137}Cs and $^{210}Pb_{xs}$, hemipelagic intervals)	Last 11.5 ± 1 ka (seismic data)
AEG02b	45	47.7 ± 4.34	12–16[a]	–	2-3	1.2 (1.0–1.5)
TRZ03	71	128.6 ± 7.07	–	1.6 (1.4–1.9)	–	No data
PSP05	77	106.5 ± 6.07	38[b]	2.8 (2.5–3.1)	–	3.3 (3.0–3.6)
PSP02	76	90.9 ± 5.14	28[c]	2.6 (2.2–2.9)	–	2.4 (2.2–2.7)

[a] From Cotteril (2006).
[b] From Beckers et al. (2015).
[c] From this study, Fig. 3C.

Please cite this article as: Beckers, A., et al., Sedimentary impacts of recent moderate earthquakes from the shelves to the basin floor in the western Gulf of Corinth, Marine Geology (2016), http://dx.doi.org/10.1016/j.margeo.2016.10.018

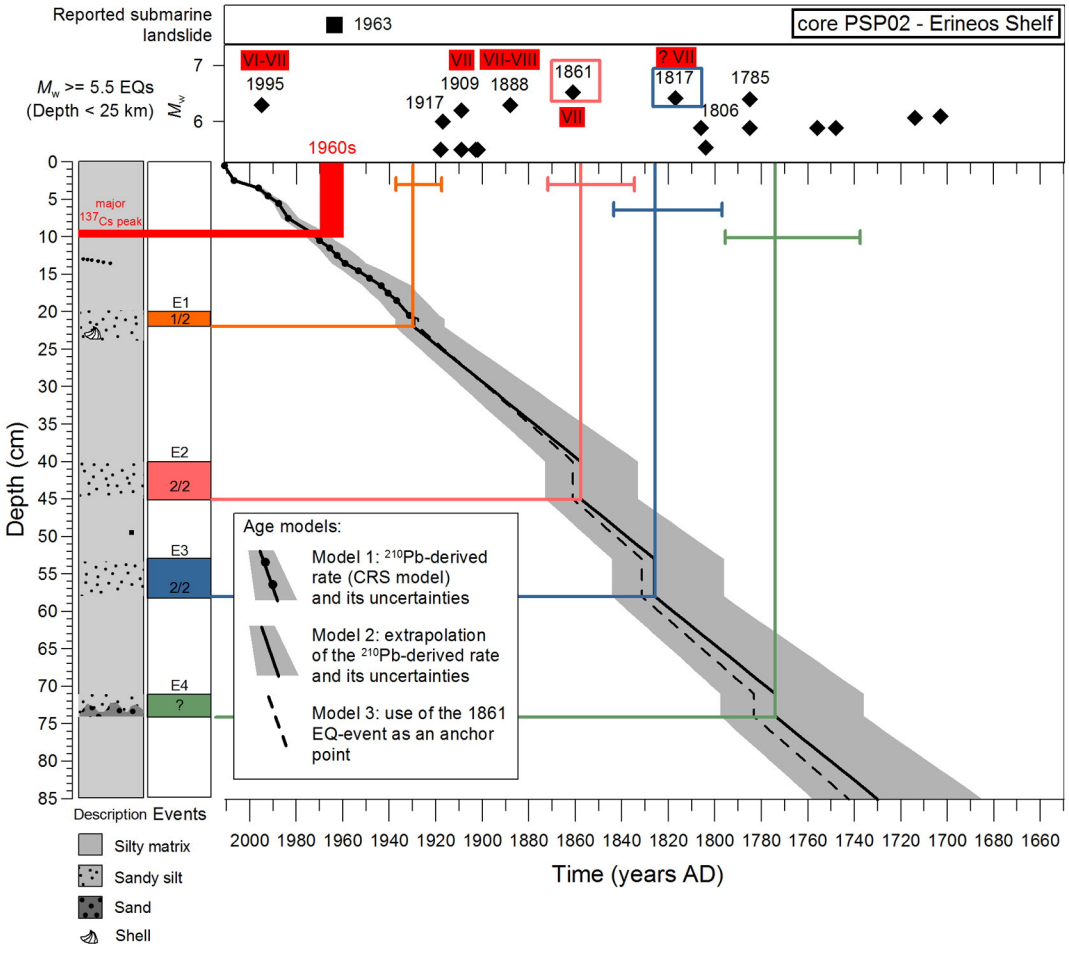

Fig. 11. Summary plot of the sedimentary record in the Erineos Shelf (left) and submarine/coastal landslides and large earthquakes reported for this area (top). The ratio mentioned for each event deposit informs about the number of cores (1 or 2) where this deposit has been recognized. In the center, 3 age-depth curves give an age to the event deposits. Roman numbers in the earthquake panel give the macroseismic intensity estimated in the sources area of the coring site from macroseismic maps (see the supplementary materials). Earthquake magnitudes from Boiselet (2014). See the text for sources of the reported submarine landslides. Boxes indicate the proposed correlations between event deposits and historical events (earthquakes or landslides).

This distinction does not apply to the basin floor coring site where only one core was retrieved (PSP05).

Concerning earthquake frequency, Table 2 shows the average recurrence time of earthquakes that were characterized by an intensity ≥ VII in the source area of each site. As mentioned earlier, this threshold is often considered in literature as being enough to trigger widespread subaqueous landslides in various settings. The proposed return periods are subjected to the likely incompleteness of the historical records. They consequently must be considered as maximum values. This concerns particularly the earthquakes of the 18th century (1785, 1756, 1748, 1714 and 1703 CE), for which only 1 to 3 MDPs are available (see the macroseismic maps in the Supplementary Materials). It has prevented us from estimating any intensity in the source areas for these earthquakes, except for the 1748 CE earthquake for which intensity VIII is given in Aigion, and thus extended to the Aigion Shelf coring site.

In the Erineos Shelf, average earthquake return period for the last 260–300 yr is close to the return period of event deposits, in the range 50–70 yr. In the Trizonia Sub-basin, for a 310–380 yr long period, the return period of event deposits is similar to the one in the Erineos Shelf, but the return period of earthquakes is longer, between 155 and 180 yr. This reflects the fact that for two earthquakes, in 1888 CE and 1817, stronger damages were reported on the southern coast than on the northern coast, and intensity VII was not reached in the northern coast (see macroseismic maps in the Supplementary Materials). In the basin floor, for a shorter period (190–270 yr), event deposits are relatively frequent (one every 27–37 yr), and average return period for strong earthquakes is relatively short (47–52 yr). The average recurrence interval of event deposits and strong earthquakes are consequently significantly different, but in the same order of magnitude. Finally, in the Aigion Shelf, the return period of earthquakes is around 40 yr, but only 3 event deposits have been found, giving an associated return period of about 57–83 yr.

At a first view, this comparison suggests that the Erineos Shelf and possibly the basin floor might preserve reliable records of past earthquakes with a local intensity larger than or equal to VII. Conversely, it seems that in the Trizonia Sub-basin and the Aigion Shelf, the correspondence between the frequencies of earthquakes and event deposits is not so good. However, the possible triggering mechanisms for each event deposit need to be discussed in order to validate this first-order comparison.

5.2. Possible impacts of earthquakes in different settings

^{210}Pb and ^{137}Cs data do not provide sufficiently accurate dating to irrefutably link an event deposit to an earthquake (Talling, 2014). Another source of age uncertainty is the problem of event deposit thickness measurement because of bioturbation, and because of the difficulty to discriminate the turbidite mud from the hemipelagic muds, as highlighted previously for the core PSP05. The assumption of a constant sedimentation rate trough time is also questionable. However, comparing temporal distributions of both phenomena is assumed here to be a good methodology to establish a causal relationship between historical

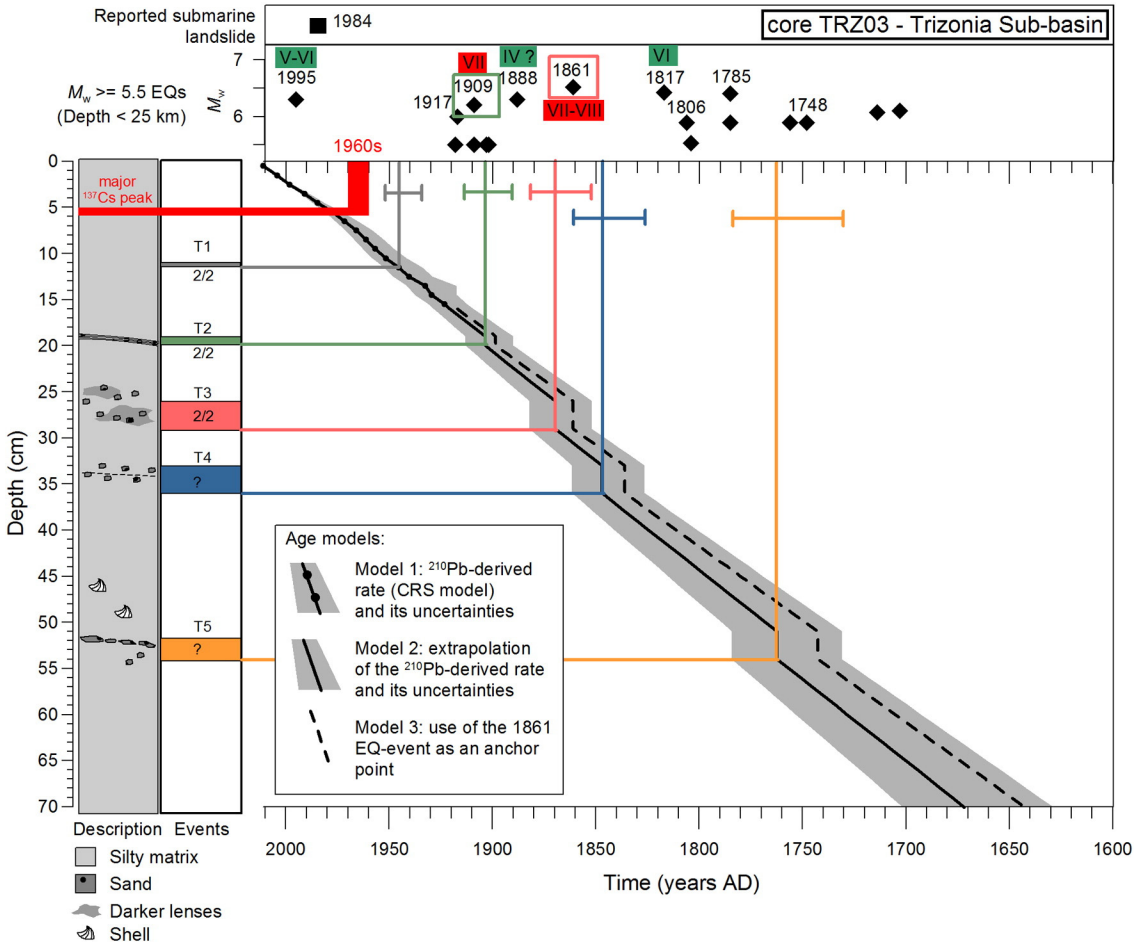

Fig. 12. Summary plot of the sedimentary record in the Trizonia Sub-basin (left) and submarine/coastal landslides and large earthquakes reported for this area (top). The ratio mentioned for each event deposit informs about the number of cores (1 or 2) where this deposit has been recognized. In the center, 3 age-depth curves give an age to the event deposits. Roman numbers in the earthquake panel give the macroseismic intensity estimated in the sources area of the coring site from macroseismic maps (see the supplementary materials). Roman numbers highlighted in red are larger than or equal to VII. Earthquake magnitude from Boiselet (2014). See the text for the sources of the reported submarine landslides. Boxes indicate the proposed correlations between event deposits and historical events (earthquakes or landslides). (For interpretation of the references to colour in this figure legend, the reader is referred to the web version of this article.)

earthquakes and event deposits (e.g. Gràcia et al., 2010; Van Daele et al., 2015).

5.2.1. Nearshore settings

Table 3 summarizes event deposit characteristics and the proposed triggers for the Aigion Shelf. At this coring site, an accurate age control is available for event deposit A1, which has been identified in the four cores. In AEG02b, the base of this event deposit is located 1 cm above the main peak in ^{137}Cs (Fig. 7), indicating an age at least younger than 1960. The main characteristic of A1 is the basal erosion highlighted by $^{210}Pb_{xs}$ data (Fig. 7). This erosion may result from oceanographic processes such as storm-wave-induced resuspension or tsunami backwash flow (e.g. Arai et al., 2013), from the passing of a sediment density flow, or from a sediment failure in the coring site area. First, erosion by storm waves seems unlikely considering the relatively reduced length of the fetch in the Gulf of Corinth and the water depth in the Aigion Shelf (40 m). Second, regarding tsunamis, three running waves have been reported in Aigion since the 1960s: in 1963 (~5 m high), 1995 (~1 m high) and 1996 (~2 m high) (Papadopoulos, 2000). Only the 1995 tsunami has been associated with an earthquake. The last event in 1996 was characterized by sea disturbances during 2 h, and left a thin sand sheet on the flooded areas (Papadopoulos, 2000), highlighting the sediment transport capacity of the waves. Regarding sediment density flows, a hyperpycnal flow coming from the Selinous River mouth, located 2 km southward, can be rejected because of the high content in shell fragments in the coarser fraction in A1. Submarine or coastal sediment failure may also evolve into a sediment density flow. In 1995, earthquake-induced coastal landslides have been reported in the Selinous delta front, essentially south of the Selinous River mouth (Fig. 2, Papatheodorou and Ferentinos, 1997). Given the morphology of the shelf, it is however unlikely that these landslides could have triggered sediment density flows reaching the coring site (Fig. 2). Finally, the 1995 earthquake – the largest earthquake to impact this site since 1909 – may have triggered sediment failures in the shelf itself. The high $^{210}Pb_{xs}$ activity in the event deposit A1 implies that A1 is not made of particles deposited on the shelf before ~1955, and possibly transported afterwards to the coring sites. This goes against a landslide origin of A1. Assuming that only one event caused the erosion at 6 cm and the deposition of A1, the previous observations lead to propose a tsunami origin for both features, which consequently occurred in 1963, 1995 or 1996. The grain size profile measured on top of AEG02, i.e. fine-grained sediments below a coarser-grained layer at the sea floor, is similar to a pre- to post-tsunami sequence described in a similar setting in Japan (Noda et al., 2007). These authors interpreted this gradient in grain-size to be the result of the erosion of small sized particles in the post-tsunami layer. This process may have played a role in the Aigion Shelf as well, but the presence of numerous shell fragments in the sandy fraction suggests that an advection of sand has occurred.

The same reasoning can be applied to the second event deposit A2. The presence of ^{137}Cs just below the event deposit indicates a deposition

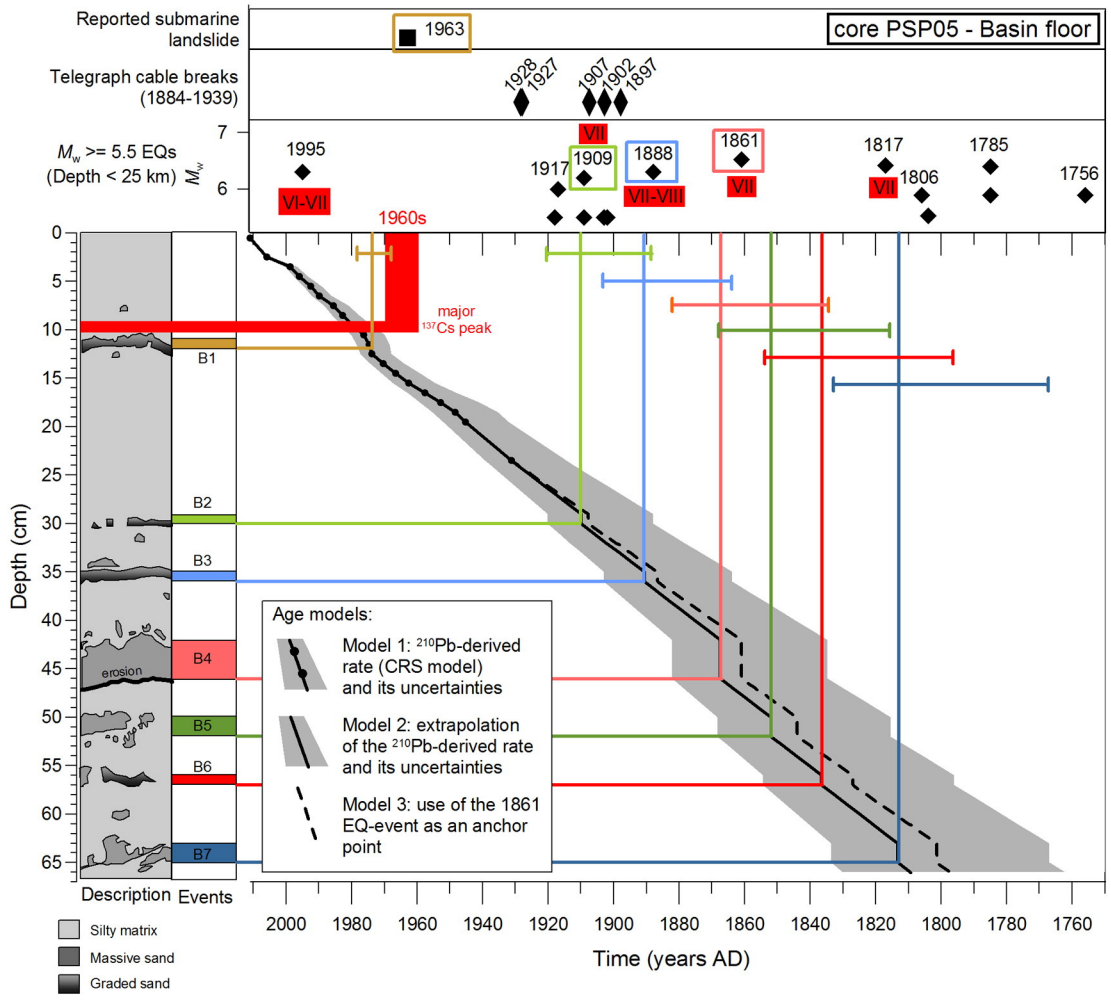

Fig. 13. Summary plot of the sedimentary record in the basin floor (left) and submarine/coastal landslides, telegraphic cable breaks and large earthquakes reported for this area (top). In the center, 3 age-depth curves give an age to the event deposits. Roman numbers in the earthquake panel give the macroseismic intensity estimated in the sources area of the coring site from macroseismic maps (see the supplementary materials). Roman numbers highlighted in red are larger than or equal to VII. Earthquake magnitude from Boiselet (2014), cable breaks from Heezen et al. (1966). See the text for the sources of the reported submarine landslides. Boxes indicate the proposed correlations between event deposits and historical events (earthquakes or landslides). (For interpretation of the references to colour in this figure legend, the reader is referred to the web version of this article.)

after 1950–1955 CE. Although XRF measurements do not highlight a change in chemical composition compared to hemipelagites, a flood origin can be rejected from the presence of shell fragments in the coarser fraction. We propose that similarly to A1, A2 results from a tsunami that hit the Aigion area after 1950, i.e. the 1963 or the 1995 tsunami.

From our rough estimate of the inter-event sedimentation rate in AEG02b, the event deposit A3 would date from 1915 to 1927. Neither strong earthquake nor tsunami has been reported during that period. The base of the core would date from 1830 CE to 1780 CE. It was expected to find in the Aigion Shelf deposits related to the 1888 CE and 1861 CE earthquakes, which both had intensities VII to VIII in the area. It is likely that a deposit related to one of these earthquakes lies a few centimeters deeper than the base of the core. Indeed, the corer has been blocked at the same depth, around 60 cm, at the sites of AEG02b, AEG03 and AEG04. This suggests that a sediment layer with different properties than the hemipelagite below A3 is located at that depth. Another coring system would be necessary to sample this likely event deposit.

In the Erineos Shelf, at least five earthquakes have induced a macroseismic intensity ≥ VII during the 260–300 yr of recorded sedimentation (Fig. 11). Because only four event deposits have been detected (summary in Table 4), the possible paleoseismological record of that site seems, if any, not complete. A first observation is that the 1995 earthquake is not recorded, despite an estimated macroseismic

Table 2
Average recurrence intervals for event deposits and strong earthquake shaking in the study sites. ED = event deposit.

Coring site	Recorded time span (years)	Number of event deposits in the "dated" core	Number of correlated event deposits	Number of estimated I ≥ VII earthquakes	Average recurrence intervals (years)	
					Event deposits	I ≥ VII earthquakes
Erineos Shelf	260–300	4	2	5	65–75	52–60
Trizonia Sub-basin	310–380	5	3	2	62–76	155–180
Basin floor	190–260	7	–	5	27–37	24–37
Aigion Shelf	170–250	3	3	4–6	57–83	~40

Table 3
Summary of observations and trigger interpretations for event deposits in the Aigion Shelf (cores AEG01, AEG02b, AEG03 and AEG04).

Event	Thickness (cm)	Number of cores where the event has been identified	Sedimentary characteristics	Interpretation (trigger, sedimentary process)
A1	1–6	3/4 or 4/4	• Peak in grain-size • Discontinuity in $^{210}Pb_{xs}$ profile • Enrichment in Zr/Rb and Ca/Fe (XRF) • Weakly blunted terrigenous grains • Many shell fragments	Tsunami back-wash sediment density flow
A2	4–7	3/4	• Two peaks in grain-size • Slump-like feature (x-rays picture) • No chemical variation (XRF) • Many shell fragments	Tsunami back-wash sediment density flow
A3	1–2	2/4	• Peak in grain-size • Enrichment in Zr/Rb and Ca/Fe (XRF)	?

intensity of VI or VII (Fig. 11). Event E1 occurred between 1916 and 1937, which does not correspond to any large earthquake or tsunami mentioned in the literature (Figs. 4 and 11). The only candidate is the M_w 6 1917 earthquake, but the epicenter was located ca. 30 km from the Erineos Shelf (Fig. 1). It implies that the local intensity, for which no information has been found, likely was relatively weak in comparison with the other earthquakes that struck the area in the 20th and 19th centuries. Given the fact that rotational slumps can affect the low-angle (0.5–2°) prodelta slopes of the western Gulf of Corinth under moderate shaking (critical earthquake ground accelerations of ~0.3 g according to Lykousis et al., 2009), the hypothesis of a triggering of E1 by the 1917 earthquake can however not be rejected. E2 is thicker than E1, and its age (1833–1873 CE) accurately corresponds to the 1861 CE earthquake, with estimated local intensity of VII. Moreover, this event is recorded in the two studied cores. This supports an earthquake trigger. This event has consequently been added in a second step in the age model in order to reduce the uncertainties for the older deposits, i.e. E3 and E4 (age model "3", Fig. 11). The transport process of E2 sediments may have been a hyperpycnal flow because of the very large part of terrestrial plants remains in the sandy fraction. It is proposed that the shaking by the A. D. 1861 earthquake may have triggered landslides onshore, providing a particularly large quantity of plant remains to the river system. Those remains might have been transported afterwards and deposited offshore. Between E1 and E2, no particular layer can be attributed to the 1909 CE or the 1888 CE earthquake, which shook the Erineos fan-delta area with an intensity of VII and VII–VIII, respectively (Fig. 11). The event deposit E3 is dated at 1796–1844 CE from the ^{210}Pb-derived model (model 2 in Fig. 11), and around 1830 CE from the model based on the 1861 earthquake (model 3). This event is recorded in the two cores. Event deposit E3 is a bit thicker than E2 and has a coarser grain-size. The part of terrigenous grains in the sandy fraction is higher than the one in E2. Assuming a small overestimation of sedimentation rates below E2, E3 reasonably fits with the 1817 CE earthquake. Indeed, we have estimated that this earthquake likely produced an intensity ≥ VIII in the Erineos Shelf area based on the few MDPs calculated in the Aigion area, which is in theory enough to trigger offshore slope failure, even on the relatively low-angle slope of the Erineos Shelf (see the stability analysis by Lykousis et al., 2009). The texture and composition of this event deposit may suggest a cohesive muddy debris flow. For the event deposit E4, age estimates (1735–1800 CE, or ca. 1780 CE) and macroseismic intensities estimates are too uncertain to discuss the possible influence of an earthquake. The very high concentration of organic remains in the coarser fraction suggests that the transport process may have been a flood, similarly to E2.

5.2.2. The Trizonia Sub-basin

In the Trizonia Sub-basin, a large-scale spatial extent is inferred for the event deposits T1, T2 and T3 from the correlation between the cores TRZ03 and TRZ04. Analyzing events deposits one by one, no detectable event deposit can again be associated with the 1995 earthquake (Fig. 12). However, this was expected from the relatively low local macroseismic intensity (V-VI) induced by that earthquake. Then, the thin turbidite T1 is dated in the range 1934–1953. This event deposit does not seem to be related to any earthquake. In 1963, the strongest rainfall for 70 years affected the area of the Gulf of Corinth and a submarine landslide-induced tsunami hit the southern and northern coasts of the western Gulf, including the source area of the Trizonia Sub-basin (Galanopoulos et al., 1964). However, radionuclide data show that T1 is at least 10 years older than 1963. This supports the inference that the triggering of this thin event deposit is independent from any known earthquake or tsunami. Conversely, the age of T2 (1890–1913) fits with the M_w 6.2 1909 earthquake whose epicentral area intersects the Trizonia Sub-basin (Ambraseys and Jackson, 1990; Supplementary materials). The estimated local macroseismic intensity reached VII. The reasoning is the same for the event deposit T3. It is dated between 1852 CE and 1882 CE, matching with the 1861 CE, M_w 6.5 earthquake.

Table 4
Summary of observations and trigger interpretations for event deposits in the Erineos Shelf (cores PSP01 and PSP02).

Event	Thickness (cm)	Number of cores where the event has been identified	Sedimentary characteristics	Interpretation (trigger, sedimentary process)
E1	2	1/2	• Peak in grain size • No chemical signature (XRF)	Not an earthquake[a], sediment failure/hyperpycnal flow
E2	4	2/2	• Sharp grain size breaks • No chemical signature (XRF) • Coarsest fraction (> 125 μm) composed of terrestrial plant remains and charcoals (~75%), forams and shell fragments (~25%)	1861 CE earthquake[a], hyperpycnal flow
E3	5	2/2	• Increase in Zr/Rb (decrease in Rb) (XRF) • Coarsest fraction (> 125 μm) composed of lithics (~75%) and terrestrial plant remains (~25%)	1817 CE earthquake, cohesive muddy debris flow
E4	3	?	• Sandy base overlain by silt • Enrichment in Pb, Fe, Br (XRF) • Coarsest fraction (> 125 μm) composed of terrestrial plant remains (~95%)	Earthquake ?, hyperpycnal flow

[a] Interpretation supported by the age of the deposit and not directly by diagnostic sedimentary characteristics.

Please cite this article as: Beckers, A., et al., Sedimentary impacts of recent moderate earthquakes from the shelves to the basin floor in the western Gulf of Corinth, Marine Geology (2016), http://dx.doi.org/10.1016/j.margeo.2016.10.018

This earthquake induced the largest macroseismic intensity at the northern side of the western Gulf for the last two centuries, with an estimated intensity of VII to VIII in the Trizonia Sub-basin area (Fig. 12).

For both event deposits T2 and T3, it is difficult to deeply discuss the sedimentary processes responsible for their transport and deposition based on the characteristics of the deposits because of the high degree of bioturbation and their small thickness. However, X-ray radiographs reveal evidences for "multipulse" events. This is an argument for the occurrence of multiple turbidity currents, coming from the different slopes surrounding the sub-basin (Goldfinger, 2011) or for a "multi-step" evolution of a unique slope failure (Talling, 2014). The first interpretation argues in favor of a synchronous trigger for each slope failure, such as an earthquake. Adding to this argument the correspondence between the ages of T2 and T3 and the 1909 and 1861 earthquakes, respectively, our analysis strongly supports an earthquake triggering for these two event deposits.

The event deposits T4 and T5 in TRZ03 are difficult to correlate with the sediment record in TRZ04 (Fig. 9). The proposed range of ages for T4 is 1856–1861 CE (model 2) or around 1840 CE if we associate T3 with the 1861 CE earthquake (model 3). Excluding the 1861 CE earthquake, this range does not fit with any known earthquake. Finally, the link between T5 and earthquake shaking is difficult to establish because of the age uncertainty for this event deposit (1731–1784 CE, or ca. 1740 CE) and the high frequency of earthquakes that occurred in that period.

In summary, the presented data suggest that in the Trizonia Sub-basin, at least two event deposits (T2 and T3) out of five could have been triggered by historical earthquakes, i.e. in 1909 and 1861 CE, respectively (Table 5). The youngest event deposit T1 very likely has not been triggered by an earthquake, and neither was T4. Triggering mechanisms for T5 are more difficult to discuss.

5.2.3. The basin floor

In PSP05 the number of event deposits (seven, their characteristics are summarized in Table 6) is larger than the number of earthquakes with an estimated intensity ≥ VII in the recorded timespan (at least four to five) (Fig. 13). As in the Trizonia Sub-basin, the 1995 earthquake did not trigger any detectable event deposit in this core. Conversely, the age of the upper event deposit B1 (1968–1977) does not fit with any earthquake retained in our catalogue. The only candidates are the two 1965 earthquakes, whose estimated intensities are smaller than VII (see the macroseismic map in the Supplementary Materials). The main shock was M_w 6.8, but occurred at a depth of 55 km. This is why this event was not in our selection. A large aseismic coastal landslide occurred two years before, in 1963, in the Erineos fan-delta. This landslide reached the basin floor, and the main associated MTD is located ca. 3 km east of the coring site (Fig. 2). Even if 1963 is out of the range of ages proposed for B1 by a tiny margin, the hypothesis that B1 is a turbidite resulting from the 1963 Erineos fan-delta landslide cannot be rejected. Below B1, 17 cm of hemipelagic sediments are not interrupted by any event deposits. This record fits very well to 45 years of absence of significant earthquake shaking in the source area according to the catalogue used (Fig. 13). Before that period, three I ≥ VII earthquakes occurred in a 50 yr long period (1909, 1888 and 1861 CE). Despite uncertainties in age, the mean age values for B2 (1909 CE), B3 (1891 CE) and B4 (1867 CE) correctly fit with the ages of these three earthquakes (Fig. 13). The event deposit B4 is proposed to be associated with the 1861 CE earthquake and is the thickest event deposit in this core. Using B4 as an anchor point reduces the age uncertainty for B1, B2 and B3, and reinforces the interpretation that B2 and B3 were triggered by the 1909 CE and 1888 CE earthquakes (model 3, Fig. 13). The integration of cable break data, however, challenges this interpretation for the event deposit B2. Indeed, three cable breaks in 1897, 1902 and 1907 CE are located in the source area of the core PSP05 and attest the occurrence of aseismic sediment density flow that could also correspond the B2 (Figs. 2 and 13).

By its sedimentological characteristics (massive terrigenous clean sand bed, sharp upper and lower contacts), B4 can be related to the 6–10 cm thick basin-wide sandy deposit described 4 km to the east in the Delphic Plateau, at 27–32 cm below the sea floor (Lykousis et al., 2007). These authors proposed that it is a tsunami deposit or the distal member of a debris flow. Based on ^{210}Pb data, they suggested that it resulted from the 1861 CE earthquake, which is consistent with our interpretation. Brought together with Lykousis et al. 's (2007) results, our data shows that this deposit could extend at least along 10 km in the basin floor. In PSP05, the base of B4 is erosional, implying an underevaluated age for B5, B6 and B7. Independently from this issue, these 3 deposits are too close in depth to each other to correspond to the last 3 major earthquakes of the studied period (1817, 1785 and 1756 CE). A sedimentation rate smaller than the present-day one is needed to establish such a correlation. In absence of evidence, this hypothesis of an increase in sedimentation rate after 1861 remains speculative. In summary, the presented data suggests that at least 3 out of 4 event deposits since 1861 were triggered by an earthquake. The low degree of bioturbation down to E4 allowed to accurately measure the thickness of each event deposit, which in turns strengthen the proposed age-depth curve and the interpretation that came out.

6. Discussion

Based on the presented results, it is possible to discuss the potential of different marine settings for off-fault paleoseismology. The sedimentary environments that have been investigated here, in the western Gulf of Corinth, differ from those usually chosen in subaqueous paleoseismology studies. For example, in marine environments, deep-water channel systems (>2000 m) often are selected with the aim of identifying turbidites that are not related to nearshore processes like storms, river floods, etc. (e.g. Goldfinger, 2011; Pouderoux et al., 2012; Ratzov et al., 2015). In lakes, sites located close to river mouths or

Table 5
Summary of observations and trigger interpretations for event deposits in the Trizonia Sub-basin (cores TRZ03 and TRZ04).

Event	Thickness (cm)	Number of cores where the event has been identified	Sedimentary characteristics	Interpretation (trigger, sedimentary process)
T1	~1	2/2	• Peak in grain size • No visible structure	Not an earthquake[a]
T2	0.2	2/2	• Multiple coarser-grained layers (x-ray picture)	1909 CE earthquake[a], sediment failure
T3	5	2/2	• Multiple coarser-grained layers (x-ray picture) • Darker convoluted lenses • Sand « clasts » • Bioturbation • Excess in Zr/Rb (XRF)	1861 CE earthquake[a], sediment failure
T4	3	1/2 or 2/2	• Multiple sandy layers (3 to 4) • Sand « clasts »	Not an earthquake[a], sediment failure
T5	0.2–0.3	1/2 or 2/2	• Fine-sand normally graded layer • Excess in Zr/Rb (XRF)	Sediment failure

[a] Interpretation supported by the age of the deposit and not directly by diagnostic sedimentary characteristics.

Please cite this article as: Beckers, A., et al., Sedimentary impacts of recent moderate earthquakes from the shelves to the basin floor in the western Gulf of Corinth, Marine Geology (2016), http://dx.doi.org/10.1016/j.margeo.2016.10.018

Table 6
Summary of observations and trigger interpretations for event deposits on the basin floor (core PSP05).

Event	Thickness (cm)	Sedimentary characteristics	Interpretation (trigger, sedimentary process)
B1	1.5	• Normally graded sandy layer • Enrichment in Zr/Rb and Cu (XRF) • Low $^{210}Pb_{XS}$ activity	Aseismic coastal slump in 1963 CE[a]
B2	0.5–1	• Normally graded silt layer	Probably the 1909 CE earthquake[a], sediment failure
B3	0.5–1	• Sandy layer, unclear grading • Sand "clasts" on top • No clear XRF signature	1888 CE earthquake[a], sediment failure
B4	4	• Massive, well sorted sand bed, normal grading • Erosive base • Sand "clasts" at the upper boundary • Enrichment in Zr/Rb and Cu (XRF)	1861 CE earthquake[a], sediment failure
B5	~2	• Irregular shape • Sandy layer • Enrichment in Zr/Rb (XRF)	Unknown trigger, slope failure
B6	~1	• Irregular shape • Finer-grained layer • Inverse + normal grading	Flood, hyperpycnal flow (?)
B7	0.2–3	• Irregular shape (convoluted structure) • Massive sand • Sharp base and sharp upper boundary (grain-size breaks)	Slope failure ?

[a] Interpretation supported by the age of the deposit and not directly by diagnostic sedimentary characteristics.

downstream steep river deltas often are avoided for the same reasons (e.g. Strasser et al., 2006; Hubert-Ferrari et al., 2012; Van Daele et al., 2015). This study focuses on sites characterized by water depths that are between those usually selected in marine and lacustrine studies. Moreover, rivers come out in the study area so that processes like hyperpycnal flows cannot be a priori disregarded. Consequently, the presented results can be used to discuss fundamental questions in paleoseismology such as the completeness of the earthquake record or the selection of the best coring location in the framework of this specific sedimentary environment.

6.1. Are we missing earthquakes in the offshore sedimentary record?

The completeness of the earthquake records is a fundamental problem in paleoseismology. This issue can be discussed for the three sites where age-depth curves have been built (Erineos Shef, Trizonia Sub-basin and basin floor). Because the uncertainties in the age-depth curves increase with depth, we only discuss the completeness of the record for the period 1850–2011 CE. During this period, three earthquakes with an estimated local intensity ≥ VII are probably missing in some coring sites: the 1995, the 1909 and the 1888 earthquakes.

The hypocenter of the M_w 6.2 1995 Aigion earthquake has been located in the region of Eratini, on the northern coast of the Gulf, at a centroidal depth of 7.2 km (Bernard et al., 1997; Fig. 1). Presented sedimentological data show that this earthquake may only have been recorded in the Aigion Shelf, in the form of a tsunami backwash-flow deposit. Considering the magnitude, location and depth, this earthquake was expected to impact the other sites as well. Indeed, Papazachos and Papaioannou's (1997) attenuation model gives an intensity of VII for all the source areas considered in this study. But the observed macroseismic intensities reveal that the model underestimated the attenuation of seismic waves for that earthquake, and consequently overestimates the macroseismic intensity by about one degree in the source areas (see the macroseismic map in the Supplementary Materials). It is consequently likely that, at these three locations, the 1995 earthquake did not trigger strong enough shaking to produce widespread offshore slope failures. The case of the 1995 earthquake highlights the importance of first using observed macroseismic intensity data, if they are available, to discuss the impact of historical earthquakes on sediment failures, rather than using an attenuation model.

The only site where other earthquakes considered as "strong" in this study are very likely missing is the Erineos Shelf. There, no event deposit is associated with the 1909 CE earthquake (local intensity VII) or the 1888 CE earthquake (local intensity VII–VIII). As proposed above, this suggests that the Erineos Shelf does not contain a complete sequence of past earthquakes. The reasons for this are discussed below.

Finally, in the Aigion Shelf, some earthquakes are definitely missing in the sediment record (cfr. Table 2), but this cannot be discussed in detail in absence of a reliable age-depth curve.

6.2. Impacts of earthquakes in different settings

The quality of the possible earthquake records differs between the coring sites. The Aigion Shelf appears as not appropriate because of the difficulty to decipher possible event deposits from the background sedimentation, the difficulty to establish a reliable age-depth curve, and the incompleteness of the record. The sedimentary record is clearer in the Erineos Shelf, but the two retrieved cores did not reveal a complete record of I ≥ VII earthquakes, like in the Aigion Shelf. Either some of these earthquakes did not trigger any sediment density flow, or the associated deposits do not have a wide spatial extent or have been eroded. In general, shelf environments are characterized by a discontinuous sedimentation influenced by river floods and oceanic processes (Addington et al., 2007; Kniskern et al., 2010). When marine currents are present, erosion may occur frequently (Carlin and Dellapenna, 2014). Shelves consequently may not be the best suitable setting for paleoseismology, even if they could potentially record back-wash flow tsunami deposits associated with earthquakes. It is also obvious that the absence of steep slopes reduces the probability of a sediment failure in shelf environments.

In deeper settings (Trizonia Sub-basin and basin floor), the record seems more complete, and age-depth curves are easier to develop with short-lived radionuclides. The deepest site, PSP05, appears to show the best record in terms of event thickness, quality of the age-depth curve, and completeness of the possible earthquake records. Events consist of terrigenous sandy layers and likely result from sediment density flows stemming from slope failures on the flanks of large Gilbert fan-deltas, e.g. the Mornos and the Erineos fan-deltas, where such terrigenous sands are available. The post-1850 event deposit record fits with the I ≥ VII earthquake series, except for one event (B1) that probably occurred aseismically. The case of the event deposit B2 is also problematic because it could either have been triggered by the 1909 earthquake, or result from an aseismic sediment density flow known from the cable break record. More cores are needed to check the spatial extent of the deposits and to highlight possible differences between earthquake-triggered and non-earthquake-triggered event

Please cite this article as: Beckers, A., et al., Sedimentary impacts of recent moderate earthquakes from the shelves to the basin floor in the western Gulf of Corinth, Marine Geology (2016), http://dx.doi.org/10.1016/j.margeo.2016.10.018

deposits. In the Trizonia Sub-basin, some event deposits likely have been triggered by historical earthquakes as well. They also consist of terrigenous sands, suggesting sediment density flows from the nearshore area. However, their very small thickness and the high degree of bioturbation make the sedimentary archive unclear. For example, some events can be missed, even using high-resolution core scanning, or mixed up with other events.

6.3. The question of sediment supply

On the basin floor, the event deposit record in PSP05 shows that the 1861, 1888, and 1909 earthquakes probably all triggered sediment density flows that deposited 1–4 cm thick sandy layers. These earthquakes were only separated by 28 and 20 years. This implies that the sediment supply around the Gulf of Corinth basin floor is sufficient to recharge the system very quickly. The occurrence of sediment failures on the foreset beds of large deltas in the southern coast during interseismic periods also points out that sediment supply is not an obstacle to the recording of earthquakes in the basin floor (e.g. Heezen et al., 1966; Lykousis et al., 2009).

On the shelves, our results show that event deposits may result from landslides that occurred onshore (E2, Erineos Shelf) or potentially from tsunamis (A1 and A2, Aigion Shelf). In such shallow-water nearshore setting, the sensibility of watersheds and coastlines to earthquake shaking and tsunamis, respectively, is consequently more likely to influence the triggering of an offshore sediment density flow than the sediment supply.

6.4. The use of the largest earthquake as an anchor point in age-depth models

We used the event deposits associated with a remarkable event (the 1861 CE earthquake, M ≈ 6.5) as an anchor point to improve the age-depth curves (model 3 in Figs. 11, 12 and 13). The risk was to fall into a circular reasoning. However, a series of arguments suggest that this approach makes sense. First, this earthquake induced a macroseismic intensity estimated ≥ VII in the source area of each coring site according to macroseismic observations (see the Supplementary Materials). Such intensities are theoretically enough to trigger widespread slope failures (e.g. Monecke et al., 2004). Second, liquefaction features and a 2 m high tsunami wave were reporting, suggesting that sediment remobilization happened (Schmidt, 1879). Finally, except for the Aigion Shelf where the corer likely did not reach a sufficient depth, an event deposit has been observed in each core at a depth that corresponds to the age of this earthquake. Consequently, this hypothesis may be considered as reasonable. Figs. 11, 12 and 13 show that including this anchor point does not improve the possible association between event deposits and earthquakes for the period before 1861. This may be due to a change in the sedimentation rate, which is difficult to constrain for this time period. However, for the sediments deposited after 1861 in the basin floor, the improved age-depth curve allows to reduce the age uncertainty for 3 events, showing that 2 of them accurately fit temporally with two earthquakes. The use of such an anchor point may be consequently considered as reasonable in some settings to reduce the uncertainty in the age of the sediments, particularly in the case of a well-known historical earthquake during which widespread geological effects (slope failures, liquefaction, etc.) have been reported.

7. Conclusion and perspective

Event deposits have been identified in different settings in the western Gulf of Corinth over a period of 170 to 380 yr. Their possible link with the high seismicity of the area and the frequent tsunamis has been investigated. In nearshore settings (40 to 100 m deep), event deposits consist of sandy silt layers. The coarser fraction is made of terrigenous grains and shell fragments (Aigion Shelf) or fragments of terrestrial organic matter (Erineos Shelf). The ages of some events fit with strong historical earthquakes and tsunamis but the record is either incomplete, or difficult to interpret because of an irregular sedimentation rate. In the 180 m deep Trizonia Sub-basin, some thin, highly bioturbated terrigenous sandy layers may correspond to turbidity currents triggered by I ≥ VII earthquakes in 1909 CE and 1861 CE. However, the high degree of bioturbation probably prevents the identification of all events. In the basin floor, event deposits are thicker and are easier to count and measure. They consist of graded or massive terrigenous sand layers. Since ~1850 CE, all but one events match with historical earthquakes, and no earthquake with an intensity ≥ VII is missing in the record.

These results show that frequent moderate earthquakes (M_w 5.8–6.5) have impacted the sedimentation in the Gulf of Corinth basin floor through the triggering of sediment density flows. The basin floor seems consequently appropriate for longer-term paleoseismological studies, even if some sandy layers may also result from aseismic sediment density flows. Conversely, nearshore settings are less favorable to paleoseismology. These environments were investigated for their potential record of tsunami back-wash sediment flows, but it has not been possible to find any clear sedimentary record of all historical tsunamis in the investigated cores.

In order to strengthen the conclusions of this research, more cores are needed in the Gulf of Corinth basin floor to investigate the spatial extent of the deposits, the corresponding volumes and the possible source areas. This will help to unravel the sediment transport processes and the triggering mechanisms involved, i.e. earthquake-triggered vs. aseismic slope failures. Such investigations are required if we want to use sediment density flow deposits in the basin floor as a reliable paleoseismological record for the Corinth Rift.

Macroseismic maps from the literature that have been used in this study. Supplementary data associated with this article can be found in the online version, at doi: 10.1016/j.margeo.2016.10.018.

Acknowledgments

This work has been carried out in the framework of the French ANR SISCOR project. Arnaud Beckers PhD grant has been funded by the Belgian FRIA. We warmly thank Pascal Bernard who developed and led the SISCOR project, as well as all the SISCOR scientific team. We also thank Koen de Rycker, Willem Versteeg, Pascale Bascou, and the crew of the R/V Alkyon for the coring campaign in 2011. Finally, we thank Jasper Moernaut and Rebecca Bell for their detailed and constructive review of the manuscript.

References

Addington, L.D., Kuehl, S.A., McNinch, J.E., 2007. Contrasting modes of shelf sediment dispersal off a high-yield river: Waiapu River, New Zealand. Mar. Geol. 243:18–30. http://dx.doi.org/10.1016/j.margeo.2007.04.018.

Albini, P., Rovida, A., Locati, M., Vigano, D., 2014. Review of Major Earthquakes in the Western Gulf of Corinth, unpublished report for the SISCOR project.

Alonso-Hernandez, C.M., Diaz-Asencio, M., Munoz-Caravaca, A., Delfanti, R., Papucci, C., Ferretti, O., Crovato, C., 2006. Recent changes in sedimentation regime in Cienfuegos Bay, Cuba, as inferred from ^{210}Pb and ^{137}Cs vertical profiles. Cont. Shelf Res. 26: 153–167. http://dx.doi.org/10.1016/j.csr.2005.08.026.

Ambraseys, N.N., 2006. Comparison of frequency of occurrence of earthquakes with slip rates from long-term seismicity data: the cases of Gulf of Corinth, Sea of Marmara and Dead Sea Fault Zone. Geophys. J. Int. 165:516–526. http://dx.doi.org/10.1111/j.1365-246X.2006.02858.x.

Ambraseys, N.N., Jackson, J.a., 1990. Seismicity and associated strain of central Greece between 1890 and 1988. Geophys. J. Int. 101, 663–708.

Appleby, P.G., Oldfield, F., 1978. The calculation of lead-210 dates assuming a constant rate of supply of unsupported ^{210}Pb to the sediment. Catena 5, 1–8.

Appleby, P.G., Oldfield, F., 1983. The assessment of ^{210}Pb data from sites with varying sediment accumulation rates. Hydrobiologica.

Arai, K., Naruse, H., Miura, R., Kawamura, K., Hino, R., Ito, Y., Inazu, D., Yokokawa, M., Izumi, N., Murayama, M., Kasaya, T., 2013. Tsunami-generated turbidity current of the 2011 Tohoku-Oki earthquake. Geology 41, 1195–1198.

Armijo, R., Meyer, B., King, G.C.P., Rigo, A., Papanastassiou, D., 1996. Quaternary evolution of the Corinth Rift and its implications for the late Cenozoic evolution of the Aegean. Geophys. J. Int. 126, 11–53.

Armijo, R., Flerit, F., King, G., Meyer, B., 2004. Linear elastic fracture mechanics explains the past and present evolution of the Aegean. Earth Planet. Sci. Lett. 217:85–95. http://dx.doi.org/10.1016/S0012-821X(03)00590-9.

Atwater, B.F., Carson, B., Griggs, G.B., Johnson, H.P., Salmi, M.S., 2014. Rethinking turbidite paleoseismology along the Cascadia subduction zone. Geology 42:827–830. http://dx.doi.org/10.1130/G35902.1.

Avallone, A., Briole, P., Agatza-balodimou, A.M., Billiris, H., Charade, O., Mitsakaki, C., Nercessian, A., Papazissi, K., Paradissis, D., Veis, G., 2004. Analysis of eleven years of deformation measured by GPS in the Corinth Rift Laboratory area. Compt. Rendus Geosci. 336:301–311. http://dx.doi.org/10.1016/j.crte.2003.12.007.

Beck, C., Mercier de Lepinay, B., Schneider, J.-L., Cremer, M., Cagatay, N., Wendenbaum, E., Boutareaud, S., Ménot, G., Schmidt, S., Weber, O., Eris, K., Armijo, R., Meyer, B., Pondard, N., Gutscher, M.-A., Turon, J.-L., Labeyrie, L., Cortijo, E., Gallet, Y., Bouquerel, H., Gorur, N., Gervais, A., Castera, M.-H., Londeix, L., de Rességuier, A., Jaouen, A., 2007. Late Quaternary co-seismic sedimentation in the Sea of Marmara's deep basins. Sediment. Geol. 199:65–89. http://dx.doi.org/10.1016/j.sedgeo.2005.12.031.

Beck, C., Campos, C., Eris, K.K., Cagatay, N., Mercier de Lepinay, B., Jouanne, F., 2015. Estimation of successive coseismic vertical offsets using coeval sedimentary events - application to the southwestern limit of the Sea of Marmara's Central Basin (North Anatolian Fault). Nat. Hazards Earth Syst. Sci. 15:247–259. http://dx.doi.org/10.5194/nhess-15-247-2015.

Beckers, A., Hubert-Ferrari, A., Beck, C., Bodeux, S., Tripsanas, E., Sakellariou, D., De Batist, M., 2015. Active faulting at the western tip of the Gulf of Corinth, Greece, from high-resolution seismic data. Mar. Geol. 360, 55–69.

Beckers, A., Beck, C., Hubert-Ferrari, A., Tripsanas, E., Crouzet, C., Sakellariou, D., Papatheodorou, G., De Batist, M., 2016. Influence of bottom currents on the sedimentary processes at the western tip of the Gulf of Corinth, Greece. Mar. Geol. 378, 312–332.

Bell, R.E., McNeill, L.C., Bull, J.M., Henstock, T.J., Collier, R.E.L., Leeder, M.R., 2009. Fault architecture, basin structure and evolution of the Gulf of Corinth Rift, central Greece. Basin Res. 21:824–855. http://dx.doi.org/10.1111/j.1365-2117.2009.00401.x.

Bell, R.E., McNeill, L.C., Henstock, T.J., Bull, J.M., 2011. Comparing extension on multiple time and depth scales in the Corinth Rift, Central Greece. Geophys. J. Int. 186, 463–470.

Bernard, P., Briole, P., Meyer, B., Lyon-Caen, H., Gomez, J.-M., Tiberi, C., Berge, C., Cattin, R., Hatzfeld, D., Lachet, C., Lebrun, B., Deschamps, A., Courboulex, F., Larroque, C., Rigo, A., Massonnet, D., Papadimitriou, P., Kassaras, J., Diagourtas, D., Makropoulos, K., Veis, G., Papazissi, K., Mitsakaki, C., Karakostas, V., Papadimitriu, E., Papanastassiou, D., Chouliaras, G., Stavrakakis, G., 1997. The Ms = 6.2, June 15, 1995 Aigion earthquake (Greece): evidence for low angle normal faulting in the Corinth rift. J. Seismol. 1, 131–150.

Bernard, P., Lyon-Caen, H., Briole, P., Deschamps, A., Boudin, F., Makropoulos, K., Papadimitriou, P., Lemeille, F., Patau, G., Billiris, H., Paradissis, D., Papazissi, K., Castarède, H., Charade, O., Nercessian, A., Avallone, A., Pacchiani, F., Zahradnik, J., Sacks, S., Linde, A., 2006. Seismicity, deformation and seismic hazard in the western rift of Corinth: new insights from the Corinth Rift Laboratory (CRL). Tectonophysics 426:7–30. http://dx.doi.org/10.1016/j.tecto.2006.02.012.

Binford, M.W., Kahl, J.S., Norton, S.a., 1993. Interpretation of ^{210}Pb profiles and verification of the CRS dating model in PIRLA project lake sediment cores. J. Paleolimnol. 9: 275–296. http://dx.doi.org/10.1007/BF00677218.

Boiselet, A., 2014. Cycle sismique et aléa sismique d'un réseau de failles actives: le cas du rift de Corinthe (Grèce). (PhD Thesis). Ecole Normale Supérieure of Paris.

Briole, P., Rigo, A., Lyon-Caen, H., Ruegg, J.C., Papazissi, K., Mitsakaki, C., Balodimou, A., Veis, G., Hatzfeld, D., Deschamps, A., 2000. Active deformation of the Corinth rift, Greece: results from repetead Global Positioning System surveys between 1990 and 1995. J. Geophys. Res. 105, 25605–25625.

Campos, C., Beck, C., Crouzet, C., Carrillo, E., Welden, A.V., Tripsanas, E., 2013a. Late Quaternary paleoseismic sedimentary archive from deep central Gulf of Corinth: time distribution of inferred earthquake-induced layers. Ann. Geophys. 56:1–15. http://dx.doi.org/10.4401/ag-6226.

Campos, C., Beck, C., Crouzet, C., Demory, F., Van Welden, A., Eris, K., 2013b. Deciphering hemipelagites from homogenites through anisotropy of magnetic susceptibility. Paleoseismic implications (Sea of Marmara and Gulf of Corinth). Sediment. Geol. 292:1–14. http://dx.doi.org/10.1016/j.sedgeo.2013.03.015.

Carlin, J.A., Dellapenna, T.M., 2014. Event-driven deltaic sedimentation on a low-gradient, low-energy shelf: the Brazos River subaqueous delta, northwestern Gulf of Mexico. Mar. Geol. 353:21–30. http://dx.doi.org/10.1016/j.margeo.2014.03.017.

Croudace, I.W., Rindby, A., Rothwell, R.G., 2006. ITRAX: description and evaluation of a new multi-function X-ray core scanner. Geol. Soc. Lond., Spec. Publ. 267:51–63. http://dx.doi.org/10.1144/GSL.SP.2006.267.01.04.

Dawson, A.G., Stewart, I., 2007. Tsunami deposits in the geological record. Sediment. Geol. 200:166–183. http://dx.doi.org/10.1016/j.sedgeo.2007.01.002.

De Martini, P.M., Pavlopoulos, K., Pantosti, D., Palyvos, N., 2007. 3HAZ Corinth Deliverable 73: dating of paleo-tsunamis (Roma).

Donadini, F., Korte, M., Constable, C.G., 2009. Geomagnetic field for 0–3 ka: 1. New data sets for global modeling. Geochem. Geophys. Geosyst. 10. http://dx.doi.org/10.1029/2008GC002295.

Donato, S.V., Reinhardt, E.G., Boyce, J.I., Rothaus, R., Vosmer, T., 2008. Identifying tsunami deposits using bivalve shell taphonomy. Geology 36:199. http://dx.doi.org/10.1130/G24554A.1.

Drab, L., Hubert Ferrari, A., Schmidt, S., Martinez, P., 2012. The earthquake sedimentary record in the western part of the Sea of Marmara, Turkey. Nat. Hazards Earth Syst. Sci. 12:1235–1254. http://dx.doi.org/10.5194/nhess-12-1235-2012.

Evangeliou, N., Florou, H., Kritidis, P., 2013. A survey of ^{137}Cs in sediments of the Eastern Mediterranean marine environment from the pre-Chernobyl age to the present. Environ. Sci. Technol. Lett. 1, 102–107.

Ferentinos, G., Brooks, M., Doutsos, T., 1985. Quaternary tectonics in the Gulf of Patras, western Greece. J. Struct. Geol. 7, 713–717.

Flotté, N., Sorel, D., Müller, C., Tensi, J., 2005. Along strike changes in the structural evolution over a brittle detachment fault: example of the Pleistocene Corinth-Patras rift (Greece). Tectonophysics 403:77–94. http://dx.doi.org/10.1016/j.tecto.2005.03.015.

Galanopoulos, A., Delimbasis, N.D., Comninakis, P.E., 1964. A tsunami generated by a slide without a seismic shock. Geol. Chron. Greece 16, 93–110.

Goldfinger, C., 2009. Sub-aqueous paleoseismology. In: McCalpin, J.P. (Ed.), Paleoseismology. Elsevier Inc.:pp. 119–170 http://dx.doi.org/10.1016/S0074-6142(09)95050-1.

Goldfinger, C., 2011. Submarine paleoseismology based on turbidite records. Annu. Rev. Mar. Sci. 3:35–66. http://dx.doi.org/10.1146/annurev-marine-120709-142852.

Gràcia, E., Vizcaino, A., Escutia, C., Asioli, A., Rodés, Á., Pallàs, R., Garcia-Orellana, J., Lebreiro, S., Goldfinger, C., 2010. Holocene earthquake record offshore Portugal (SW Iberia): testing turbidite paleoseismology in a slow-convergence margin. Quat. Sci. Rev. 29:1156–1172. http://dx.doi.org/10.1016/j.quascirev.2010.01.010.

Hatzfeld, D., Karakostas, V., Ziazia, M., Kassaras, I., Papadimitriou, E., Makropoulos, K., Voulgaris, N., Papaioannou, C., 2000. Microseismicity and faulting geometry in the Gulf of Corinth (Greece). Geophys. J. Int. 141:438–456. http://dx.doi.org/10.1046/j.1365-246x.2000.00092.x.

Heezen, B.C., Ewing, M., Johnson, G.L., 1966. The Gulf of Corinth floor. Deep Res. 13, 381–411.

Hubert-Ferrari, A., King, G., Manighetti, I., Armijo, R., Meyer, B., Tapponnier, P., 2003. Long-term elasticity in the continental lithosphere; modelling the Aden Ridge propagation and the Anatolian extrusion process. Geophys. J. Int. 153:111–132. http://dx.doi.org/10.1046/j.1365-246X.2003.01872.x.

Hubert-Ferrari, A., Avsar, U., El Ouahabi, M., Lepoint, G., Martinez, P., Fagel, N., 2012. Paleoseismic record obtained by coring a sag-pond along the North Anatolian Fault (Turkey). Ann. Geophys. 55. http://dx.doi.org/10.4401/ag-5460.

Jolivet, L., 2001. A comparison of geodetic and finite strain pattern in the Aegean, geodynamic implications. Earth Planet. Sci. Lett. 187, 95–104.

Jolivet, L., Labrousse, L., Agard, P., Lacombe, O., Bailly, V., Lecomte, E., Mouthereau, F., Mehl, C., 2010. Rifting and shallow-dipping detachments, clues from the Corinth Rift and the Aegean. Tectonophysics 483:287–304. http://dx.doi.org/10.1016/j.tecto.2009.11.001.

Jonathan, M.P., Srinivasalu, S., Thangadurai, N., Rajeshwara-Rao, N., Ram-Mohan, V., Narmatha, T., 2012. Offshore depositional sequence of 2004 tsunami from Chennai, SE coast of India. Nat. Hazards 62:1155–1168. http://dx.doi.org/10.1007/s11069-012-0141-5.

Kagan, E., Stein, M., Agnon, A., Neumann, F., 2011. Intrabasin paleoearthquake and quiescence correlation of the late Holocene Dead Sea. J. Geophys. Res. 116, B04311. http://dx.doi.org/10.1029/2010JB007452.

Kniskern, T.A., Kuehl, S.A., Harris, C.K., Carter, L., 2010. Sediment accumulation patterns and fine-scale strata formation on the Waiapu River shelf, New Zealand. Mar. Geol. 270:188–201. http://dx.doi.org/10.1016/j.margeo.2008.12.003.

Kokkalas, S., Xypolias, P., Koukouvelas, I., Doutsos, T., 2006. Postcollisional contractional and extensional deformation in the Aegean region. Spec. Pap. Geol. Soc. Am. 409, 97–123.

Kontopoulos, N., Avramidis, P., 2003. A late Holocene record of environmental changes from the Aliki lagoon, Egion, North Peloponnesus, Greece. Quat. Int. 111:75–90. http://dx.doi.org/10.1016/S1040-6182(03)00016-8.

Kortekaas, S., Papadopoulos, G.a., Ganas, A., Cundy, A.B., Diakantoni, A., 2011. Geological identification of historical tsunamis in the Gulf of Corinth, Central Greece. Nat. Hazards Earth Syst. Sci. 11:2029–2041. http://dx.doi.org/10.5194/nhess-11-2029-2011.

Koukouvelas, I.K., Stamatopoulos, L., Katsonopoulou, D., Pavlides, S., 2001. A palaeoseismological and geoarchaeological investigation of the Eliki fault, Gulf of Corinth, Greece. J. Struct. Geol. 23:531–543. http://dx.doi.org/10.1016/S0191-8141(00)00124-3.

Koukouvelas, I.K., Katsonopoulou, D., Soter, S., Xypolias, P., 2005. Slip rates on the Helike Fault, Gulf of Corinth, Greece: new evidence from geoarchaeology. Terra Nova 17: 158–164. http://dx.doi.org/10.1111/j.1365-3121.2005.00603.x.

Lambotte, S., Lyon-Caen, H., Bernard, P., Deschamps, A., Patau, G., Nercessian, A., Pacchiani, F., Bourouis, S., Drilleau, M., Adamova, P., 2014. Reassessment of the rifting process in the Western Corinth Rift from relocated seismicity. Geophys. J. Int. 197:1822–1844. http://dx.doi.org/10.1093/gji/ggu096.

Leeder, M.R., Portman, C., Andrews, J.E., Collier, R.E.L., Finch, E., Gawthorpe, R.L., McNeill, L.C., Pérez-Arlucea, M., Rowe, P., 2005. Normal faulting and crustal deformation, Alkyonides Gulf and Perachora peninsula, eastern Gulf of Corinth rift, Greece. J. Geol. Soc. Lond. 162, 549–561.

Lurcock, P.C., Wilson, G.S., 2012. PuffinPlot: a versatile, user-friendly program for paleomagnetic analysis. Geochem. Geophys. Geosyst. 13:1–6. http://dx.doi.org/10.1029/2012GC004098.

Lykousis, V., 1990. Prodelta sediments: seismic stratigraphy, sedimentology, slope stability. (PhD Thesis). University of Patras.

Lykousis, V., Sakellariou, D., Rousakis, G., Alexandri, S., Kaberi, H., Nomikou, P., Georgiou, P., Balas, D., 2007. Sediment failure processes in active grabens: the western gulf of Corinth (Greece). In: Lykousis, V., Sakellariou, D., Locat, J. (Eds.), Submarine Mass Movements and Their Consequences III. Springer, pp. 297–305.

Lykousis, V., Roussakis, G., Sakellariou, D., 2009. Slope failures and stability analysis of shallow water prodeltas in the active margins of Western Greece, northeastern Mediterranean Sea. Int. J. Earth Sci. 98:807–822. http://dx.doi.org/10.1007/s00531-008-0329-9.

Mchugh, C., Seeber, L., Cormier, M., Dutton, J., Cagatay, N., Polonia, A., Ryan, W., Gorur, N., 2006. Submarine earthquake geology along the North Anatolia Fault in the Marmara Sea, Turkey: a model for transform basin sedimentation. Earth Planet. Sci. Lett. 248: 661–684. http://dx.doi.org/10.1016/j.epsl.2006.05.038.

Please cite this article as: Beckers, A., et al., Sedimentary impacts of recent moderate earthquakes from the shelves to the basin floor in the western Gulf of Corinth, Marine Geology (2016), http://dx.doi.org/10.1016/j.margeo.2016.10.018

McNeill, L.C., Cotterill, C.J., Bull, J.M., Henstock, T.J., Bell, R., Stefatos, A., 2007. Geometry and slip rate of the Aigion fault, a young normal fault system in the western Gulf of Corinth. Geology 35:355. http://dx.doi.org/10.1130/G23281A.1.

Moernaut, J., De Batist, M., Heirman, K., Van Daele, M., Pino, M., Brümmer, R., Urrutia, R., 2009. Fluidization of buried mass-wasting deposits in lake sediments and its relevance for paleoseismology: results from a reflection seismic study of lakes Villarrica and Calafquén (South-Central Chile). Sediment. Geol. 213:121–135. http://dx.doi.org/10.1016/j.sedgeo.2008.12.002.

Moernaut, J., Van Daele, M., Heirman, K., Fontijn, K., Strasser, M., Pino, M., Urrutia, R., De Batist, M., 2014. Lacustrine turbidites as a tool for quantitative earthquake reconstruction: new evidence for a variable rupture mode in South-Central Chile. J. Geophys. Res. Solid Earth 119 (3), 1607–1633.

Monecke, K., Anselmetti, F.S., Becker, A., Sturm, M., Giardini, D., 2004. The record of historic earthquakes in lake sediments of Central Switzerland. Tectonophysics 394:21–40. http://dx.doi.org/10.1016/j.tecto.2004.07.053.

Mulder, T., Syvitski, J.P.M., Migeon, S., Faugères, J.-C., Savoye, B., 2003. Marine hyperpycnal flows: initiation, behavior and related deposits. A review. Mar. Pet. Geol. 20:861–882. http://dx.doi.org/10.1016/j.marpetgeo.2003.01.003.

Musson, R.M.W., Grünthal, G., Stucchi, M., 2010. The comparison of macroseismic intensity scales. J. Seismol. 14:413–428. http://dx.doi.org/10.1007/s10950-009-9172-0.

Noda, A., Katayama, H., Sagayama, T., Suga, K., Uchida, Y., Satake, K., Abe, K., Okamura, Y., 2007. Evaluation of tsunami impacts on shallow marine sediments: an example from the tsunami caused by the 2003 Tokachi-oki earthquake, northern Japan. Sediment. Geol. 200:314–327. http://dx.doi.org/10.1016/j.sedgeo.2007.01.010.

Palyvos, N., Pantosti, D., 2007. 3HAZ Corinth Project Deliverable 30-Maps of Active Faults, Landslides and Marine Terraces (Roma).

Pantosti, D., De Martini, P.M., Koukouvelas, I., Stamatopoulos, L., Palyvos, N., Pucci, S., Lemeille, F., S., P., 2004. Palaeoseismological investigations of the Aigion Fault (Gulf of Corinth, Greece). Compt. Rendus Geosci. 336:335–342. http://dx.doi.org/10.1016/j.crte.2003.12.005.

Papadopoulos, G.a., 2000. Historical Earthquakes and Tsunamis in the Corinth Rift, Central Greece. National Observatory of Athens, Institute of Geodynamics, Athens.

Papadopoulos, G.A., 2003. Tsunami hazard in the Eastern Mediterranean: strong earthquakes and tsunamis in the Corinth Gulf, Central Greece. Nat. Hazards 29, 437–464.

Papatheodorou, G., Ferentinos, G., 1997. Submarine and coastal sediment failure triggered by the 1995, M = 6.1 R Aegion earthquake, Gulf of Corinth, Greece. Mar. Geol. 137, 287–304.

Papazachos, C., Papaioannou, C., 1997. The macroseismic field of the Balkan area. J. Seismol. 1, 181–201.

Papazachos, B., Papazachou, C., 2003. Earthquakes of Greece, 3rd. editio. ed. Ziti publications, Thessaloniki.

Pavlides, S.B., Koukouvelas, I.K., Kokkalas, S., Stamatopoulos, L., Keramydas, D., Tsodoulos, I., 2004. Late Holocene evolution of the East Eliki fault, Gulf of Corinth (Central Greece). Quat. Int. 115-116:139–154. http://dx.doi.org/10.1016/S1040-6182(03)00103-4.

Perissoratis, C., Piper, D.J.W., Lykousis, V., 2000. Alternating marine and lacustrine sedimentation during late Quaternary in the Gulf of Corinth rift basin, central Greece. Mar. Geol. 167, 391–411.

Pérouse, E., Chamot-Rooke, N., Rabaute, A., Briole, P., Jouanne, F., Georgiev, I., Dimitrov, D., 2012. Bridging onshore and offshore present-day kinematics of central and eastern Mediterranean: implications for crustal dynamics and mantle flow. Geochem. Geophys. Geosyst. 13. http://dx.doi.org/10.1029/2012GC004289 (n/a–n/a).

Piper, D.J.W., Kontopoulos, N., Panagos, A.G., 1988. Deltaic sedimentation and stratigraphic sequences in post-orogenic basins, Western Greece. Sediment. Geol. http://dx.doi.org/10.1016/0037-0738(88)90135-2.

Piper, D.J.W., Kontopoulos, N., Anagnostou, C., Chronis, G., Panagos, A.G., 1990. Modern fan deltas in the western Gulf of Corinth, Greece. Geo-Mar. Lett. 10, 5–12.

Pouderoux, H., Lamarche, G., Proust, J.-N., 2012. Building an 18 000-year-long paleoearthquake record from detailed deep-sea turbidite characterisation in Poverty Bay, New Zealand. Nat. Hazards Earth Syst. Sci. 12:2077–2101. http://dx.doi.org/10.5194/nhess-12-2077-2012.

Ratzov, G., Cattaneo, A., Babonneau, N., Déverchère, J., Yelles, K., Bracene, R., Courboulex, F., 2015. Holocene turbidites record earthquake supercycles at a slow-rate plate boundary. Geology http://dx.doi.org/10.1130/G36170.1.

Reilinger, R., McClusky, S., Paradissis, D., Ergintav, S., Vernant, P., 2010. Geodetic constraints on the tectonic evolution of the Aegean region and strain accumulation along the Hellenic subduction zone. Tectonophysics 488:22–30. http://dx.doi.org/10.1016/j.tecto.2009.05.027.

Rigo, A., Lyon-Caen, H., Armijo, R., Deschamp, A., Hatzfeld, D., Makropoulos, K., Papadimitriou, P., Kassaras, I., 1996. A microseismic study in the western part of the Gulf of Corinth (Greece): implications for large-scale normal faulting mechanisms. Geophys. J. Int. 126, 663–688.

Roberts, P.G., Koukouvelas, I., 1996. Roberts & Koukouvelas 1996.pdf. Ann. Geofis. 39, 619–646.

Schmidt, J., 1879. Studien uber Erdbeben (Leipzig).

Schwartz, M., Tziavos, C., 1979. Geology in the search for ancient Helice. J. F. Archaeol. 6, 243–252.

Schwarz-Zanetti, G., Deichmann, N., Fäh, D., Giardini, D., Jimenez, M.-J., Masciadri, V., Schibler, R., Schnellmann, M., 2003. The earthquake in Unterwalden on September 18, 1601: a historico-critical macroseismic evaluation. Eclogae Geol. Helv. 96, 441–450.

Skourtsos, E., Kranis, H., 2009. Structure and evolution of the western Corinth Rift, through new field data from the Northern Peloponnesus. Geol. Soc. Lond., Spec. Publ. 321:119–138. http://dx.doi.org/10.1144/SP321.6.

Sokos, E., Zahradník, J., Kiratzi, A., Janský, J., Gallovič, F., Novotny, O., Kostelecký, J., Serpetsidaki, A., Tselentis, G.-A., 2012. The January 2010 Efpalio earthquake sequence in the western Corinth Gulf (Greece). Tectonophysics 530-531:299–309. http://dx.doi.org/10.1016/j.tecto.2012.01.005.

Sorel, D., 2000. A Pleistocene and still-active detachment fault and the origin of the Corinth-Patras rift, Greece. Geology 28:83–86. http://dx.doi.org/10.1130/0091-7613(2000)28<83.

Stefatos, A., Charalambakis, M., Papatheodorou, G., Ferentinos, G., 2006. Tsunamigenic sources in an active European half-graben (Gulf of Corinth, Central Greece). Mar. Geol. 232:35–47. http://dx.doi.org/10.1016/j.margeo.2006.06.004.

Stein, S., Geller, R.J., Liu, M., 2012. Why earthquake hazard maps often fail and what to do about it. Tectonophysics 562-563:1–25. http://dx.doi.org/10.1016/j.tecto.2012.06.047.

Strasser, M., Anselmetti, F.S., Fäh, D., Giardini, D., Schnellmann, M., 2006. Magnitudes and source areas of large prehistoric northern Alpine earthquakes revealed by slope failures in lakes. Geology 34:1005–1008. http://dx.doi.org/10.1130/G22784A.1.

Strasser, M., Hilbe, M., Anselmetti, F.S., 2011. Mapping basin-wide subaquatic slope failure susceptibility as a tool to assess regional seismic and tsunami hazards. Mar. Geophys. Res. 32:331–347. http://dx.doi.org/10.1007/s11001-010-9100-2.

Sumner, E.J., Siti, M.I., McNeill, L.C., Talling, P.J., Henstock, T.J., Wynn, R.B., Djajadihardja, Y.S., Permana, H., 2013. Can turbidites be used to reconstruct a paleoearthquake record for the central Sumatran margin? Geology 41:763–766. http://dx.doi.org/10.1130/G34298.1.

Talling, P.J., 2014. On the triggers, resulting flow types and frequencies of subaqueous sediment density flows in different settings. Mar. Geol. 352:155–182. http://dx.doi.org/10.1016/j.margeo.2014.02.006.

Taylor, B., Weiss, J.R., Goodliffe, A.M., Sachpazi, M., Laigle, M., Hirn, A., 2011. The structures, stratigraphy and evolution of the Gulf of Corinth rift, Greece. Geophys. J. Int. 185:1189–1219. http://dx.doi.org/10.1111/j.1365-246X.2011.05014.x.

Tema, E., Kondopoulou, D., 2011. Secular variation of the Earth's magnetic field in the Balkan region during the last eight millennia based on archaeomagnetic data. Geophys. J. Int. 186:603–614. http://dx.doi.org/10.1111/j.1365-246X.2011.05088.x.

Tinti, S., Zaniboni, F., Armigliato, A., Pagnoni, G., Gallazzi, S., Manucci, A., Brizuela Reyes, B., Bressan, L., Tonini, R., 2007. Tsunamigenic landslides in the western Corinth gulf: numerical scenarios. In: Lykousis, V., Sakellariou, D. (Eds.), Submarine Mass Movements and Their Consequences. Springer, pp. 405–414.

Tsabaris, C., Kapsimalis, V., Eleftheriou, G., Laubenstein, M., Kaberi, H., Plastino, W., 2012. Determination of ^{137}Cs activities in surface sediments and derived sediment accumulation rates in Thessaloniki Gulf, Greece. Environ. Earth Sci. 67:833–843. http://dx.doi.org/10.1007/s12665-012-1530-5.

Van Daele, M., Moernaut, J., Doom, L., Boes, E., Fontijn, K., Heirman, K., Vandoorne, W., Hebbeln, D., Pino, M., Urrutia, R., Brümmer, R., De Batist, M., 2015. A comparison of the sedimentary records of the 1960 and 2010 great Chilean earthquakes in 17 lakes: implications for quantitative lacustrine palaeoseismology. Sedimentology 62:1466–1496. http://dx.doi.org/10.1111/sed.12193.

Van Welden, A., 2007. Enregistrements sédimentaires imbriqués d'une activité sismique et de changements paléo-environnementaux. Etude comparée de différents sites: Golfe de Corinthe (Grèce), Lac de Shkodra (Alabanie/Montenegro), Golfe de Cariaco (Vénézuela). (PhD Thesis). University of Savoie.

Westaway, R., 2002. The Quaternary evolution of the Gulf of Corinth, central Greece: coupling between surface processes and flow in the lower continental crust. Tectonophysics 348, 269–318.

Wilhelm, B., Arnaud, F., Sabatier, P., Magand, O., Chapron, E., Courp, T., Tachikawa, K., Fanget, B., Malet, E., Pignol, C., Bard, E., Delannoy, J.J., 2013. Palaeoflood activity and climate change over the last 1400 years recorded by lake sediments in the northwest European Alps. J. Quat. Sci. 28:189–199. http://dx.doi.org/10.1002/jqs.2609.

Please cite this article as: Beckers, A., et al., Sedimentary impacts of recent moderate earthquakes from the shelves to the basin floor in the western Gulf of Corinth, Marine Geology (2016), http://dx.doi.org/10.1016/j.margeo.2016.10.018